Quaternary Science Reviews 288 (2022) 107572

Contents lists available at ScienceDirect

Quaternary Science Reviews

journal homepage: www.elsevier.com/locate/quascirev

Pliocene - Early Pleistocene continental climate and vegetation in Europe based on stable isotope compositions of mammal tooth enamel

Péter Szabó [a, b], János Kovács [a, b, *], László Kocsis [c], Torsten Vennemann [c], Laura Domingo [d, e], Gábor Újvári [f], Ákos Halmai [b], Ervin Pirkhoffer [b], Vlad Codrea [g]

[a] Environmental Analytical and Geoanalytical Research Group, Szentágothai Research Centre, University of Pécs, Pécs, Hungary
[b] Institute of Geography and Earth Sciences. University of Pécs, Pécs, Hungary
[c] Institute of Earth Surface Dynamics, University of Lausanne, Lausanne, Switzerland
[d] Departamento de Geodinámica, Estratigrafía y Paleontología, Facultad de Ciencias Geológicas, Universidad Complutense de Madrid, Madrid, Spain
[e] Earth and Planetary Sciences Department, University of California Santa Cruz, Santa Cruz, USA
[f] Institute for Geological and Geochemical Research, Research Centre for Astronomy and Earth Sciences, Budapest, Hungary
[g] Faculty of Biology and Geology, Babeş-Bolyai University, Cluj-Napoca, Romania

ARTICLE INFO

Article history:
Received 4 March 2022
Received in revised form
15 May 2022
Accepted 15 May 2022
Available online 2 June 2022

Handling Editor: Mira Matthews

Keywords:
Paleoclimate
Vertebrate fossils
South and central Europe

ABSTRACT

There is an increasing need for paleoclimate records from continental settings to better understand the climatic changes during critical periods such as the Pliocene and Early Pleistocene. Present data indicates a transition from a warmer than present-day climate to a substantially different cooler climate. This study reviews the oxygen and carbon isotope compositions of mammalian tooth enamel for the Pliocene and Early Pleistocene of South and Central Europe to reconstruct the spatial distribution and temporal changes of the vegetation and oxygen isotope composition of precipitation ($\delta^{18}O_{ppt}$). In addition to a literature review, this study adds new stable isotope measurements for this period. All $\delta^{13}C$ values indicate C_3 ecosystems and reflect major changes in the water use efficiency and/or in the prevailing humidity. The reconstructed major floral types range from woodland to woodland – mesic grassland in all of the investigated regions. The carbon isotope compositions of fossil mammal teeth demonstrate that the spatial distribution of vegetation was broadly similar to those of the present-day for the Early/Late Pliocene – Early Pleistocene, with the most "closed" vegetation in Central and Northern Italy, while open mesic grassland vegetation covers can be reconstructed for the Iberian Peninsula, Massif Central region (Central France) and the Carpathian Basin. The calculated $\delta^{18}O_{ppt}$ values give a negative temporal shift of about 1–1.5‰ from the Early Pliocene to Late Pliocene – Early Pleistocene in three regions (Iberian Peninsula, Central Italy, Carpathian Basin), potentially representing a 1.5–3.0 °C decrease in mean annual temperatures (MAT) over time. In the Massif Central region and the Carpathian Basin, the $\delta^{18}O_{ppt}$ values are almost the same for the Late Pliocene and Early Pleistocene, while in Northern Italy the values decreased over that period. The $\delta^{18}O_{ppt}$ values are in the range of present-day $\delta^{18}O_{ppt}$ values over the Early Pliocene and somewhat lower than present-day values for the Late Pliocene - Early Pleistocene in most of the regions. Because most other proxies indicate warmer than present-day climate for the Early Pliocene and similar to present-day climate for the Early Pleistocene, the $\delta^{18}O_{ppt}$ values are generally lower than expected, which can be partially explained by local effects.

1. Introduction

Reconstructions of paleoenvironments and paleoclimates are based on various proxies (e.g., Masson-Delmotte et al., 2013), but only a few are generally considered reliable in the terrestrial realm. Also, terrestrial climate reconstruction is often difficult because

* Corresponding author. Environmental Analytical and Geoanalytical Research Group, Szentágothai Research Centre, University of Pécs, Pécs, Hungary.
E-mail address: jones@gamma.ttk.pte.hu (J. Kovács).

https://doi.org/10.1016/j.quascirev.2022.107572

land ecosystems and climates have large spatial and temporal heterogeneities. Given that teeth and bones are usually well preserved in the fossil record, and the natural variations in stable isotope ratios of bioapatite in homeotherm/warm-blooded animals largely depend on environmental variables, the stable isotope analysis of teeth has become an indispensable and powerful tool in reconstructing changes in terrestrial paleoclimate and paleoenvironments (e.g., Sullivan and Krueger, 1981; Luz et al., 1984, 1990; Lee-Thorp and van der Merwe, 1987; Lee-Thorp et al., 1989; Ayliffe et al., 1992, 1994; Bryant and Froelich, 1995; Bocherens et al., 1996; Fricke et al., 1998; Cerling and Harris, 1999; Kohn et al., 1999; Kohn and Cerling, 2002; Arppe and Karhu, 2006; Tütken et al., 2006; Martin et al., 2008; Kohn, 2010; Pellegrini et al., 2011; Domingo et al., 2013, 2015, 2020; Kocsis et al., 2014; García-Alix, 2015; Kovács et al., 2012, 2015, 2020; Hartman et al., 2016; Metcalfe et al., 2016 and references therein).

Because the carbon stable isotope compositions ($\delta^{13}C$) of biological apatite are directly linked to the isotope compositions of the average diet of the animal ($\delta^{13}C_{diet}$), measurements of the C-isotope compositions of the bioapatite allow for a reconstruction of the vegetative cover used as a food source (e.g., Koch, 1998; Cerling and Harris, 1999; Passey et al., 2005). $\delta^{13}C_{diet}$ values can provide information about the ratio of plants using different photosynthetic pathways (C_3 and C_4 type, O'Leary, 1988; Farquhar et al., 1989; Martinelli et al., 1991), while in C_3 ecosystems information can be obtained about the vegetation "openness" (van der Merwe and Medina, 1991; Bocherens et al., 1996; Cerling and Harris, 1999; Drucker et al., 2008), relative humidity or the Mean Annual Precipitation (MAP, Kohn, 2010) and habitat differences or niche partitioning between animals (e.g., Feranec and MacFadden, 2006). The oxygen isotope composition of mammalian teeth enamel is determined by the isotopic composition of the animal's body water, which, in the case of obligate drinking large herbivores reflects mainly the ingested environmental waters (e.g., Longinelli, 1984; Luz et al., 1984; Bryant et al., 1996; Fricke and O'Neil, 1996; Fricke et al., 1998; Koch, 2007). The $\delta^{18}O$ values of meteoric water are controlled by several factors, including the Mean Annual Temperature (MAT), latitude, altitude, continental and/or amount effects (Dansgaard, 1964; Rozanski et al., 1993). At mid and high latitudes, the correlation is usually the strongest with the MAT. These correlations provide the basis for using the $\delta^{18}O$ values of tooth enamel to detect past climatic changes.

This study is aimed at reconstructing temporal changes and spatial patterns of the oxygen isotope compositions of precipitation ($\delta^{18}O_{ppt}$) using $\delta^{18}O_{PO4}$ in teeth and detecting temporal changes and the spatial distribution of vegetation and humidity based on enamel $\delta^{13}C$ values over the Pliocene and Early Pleistocene in South and Central Europe. To achieve these goals, stable isotope compositions are reviewed from the literature and complemented by further, new measurements of tooth enamel isotopic compositions from large and middle-sized mammals of the Pliocene to Early Pleistocene. New stable isotope analyses for this study were made on mammalian tooth enamel from localities situated in France, Bosnia-Hercegovina, and Romania. Existing oxygen and carbon stable isotope data of the Pliocene and Early Pleistocene are from several regions of the Iberian Peninsula, the Italian Peninsula, and the Carpathian Basin (Sánchez-Chillón et al., 1994; van Dam and Reichart, 2009; Matson and Fox, 2010; Domingo et al., 2013; Kovács et al., 2015; Johnson and Geary, 2016; Szabó et al., 2017).

2. Background

2.1. Stable carbon and oxygen isotope compositions of teeth

Tooth enamel consists almost entirely of structurally compact bioapatite (96%) with large phosphate crystallites (up to 1 μm long), which makes enamel the most resistant tissue to diagenesis compared to other osseous tissues such as bone, dentine, and cement (e.g., Kohn et al., 1999). Thus, it is one of the most likely materials to remain unaltered in the fossil record (e.g., Lee-Thorp and van der Merwe, 1987; Quade et al., 1992; Ayliffe et al., 1994; Wang and Cerling, 1994; Koch et al., 1997; Kohn et al., 1999). Mammal bioapatite is mainly hydroxyapatite with many substitutions and complex non-stoichiometric compositions. A significant amount of carbonate ions and several minor and trace elements substitute in the crystal lattice. The composition can be written in simplified form, as $Ca_{8.8}Mg_{0.1}(PO_4)_9(HPO_4)_{0.6}(CO_3)_{0.5}(OH)_{0.9}$ (Combes et al., 2016). The presence of the carbonate ions in the apatite structure allows for the measurements of the $^{13}C/^{12}C$ and $^{18}O/^{16}O$ isotopic ratios in the carbonate group. Measuring the $^{18}O/^{16}O$ isotope ratio of the phosphate group, however, has been proven to be more reliable because phosphate oxygen is more resistant to low temperature inorganic diagenetic alteration processes compared to the carbonate-bound oxygen, given the stronger P–O bonds and lower solubility of bioapatite compared to carbonate (e.g., Kohn et al., 1999; Kohn and Cerling, 2002; ; Zazzo et al., 2004a; 2004b).

2.2. Stable carbon isotope composition of enamel and diet

The carbon isotope composition of tooth enamel reflects the ingested food of mammals at the time of tooth formation. There is a 13–14‰ difference in $\delta^{13}C$ values of the enamel of large herbivores relative to that of the diet (Koch, 1998; Cerling and Harris, 1999; Passey et al., 2005), with this difference being related to body mass and physiology (Passey et al., 2005; Tejada-Lara et al., 2018). The $\delta^{13}C$ values of plants depend mostly on the photosynthetic pathway and environmental parameters, such as water availability, atmospheric CO_2 concentration, sunlight, and salinity, among others (Farquhar et al., 1989). The C_3 and C_4 photosynthetic pathways have been described for different kinds of plant groups. All trees, most shrubs and herbs, and grasses in regions with a cool-temperate growing season follow the C_3 photosynthetic pathway, with a mean $\delta^{13}C$ value of about −27‰ for their cellulose; covering a range from −35 to −22‰ (O'Leary, 1988; Farquhar et al., 1989; Ehleringer and Monson, 1993; Hayes, 2001). Grasses from regions with a warm growing and generally dry season, some sedges (Bruhl and Wilson, 2007), and dicots use the C_4 photosynthetic pathway. C_4 plants have higher $\delta^{13}C$ values with a mean value of about −13‰ and a range between −19 and −9‰ (O'Leary, 1988; Farquhar et al., 1989; Ehleringer and Monson, 1993; Hayes, 2001). In C_3 ecosystems, the $\delta^{13}C$ values increase with decreasing mean annual precipitation (MAP) (Kohn, 2010), decreasing humidity, and increasing availability of light. Herbs and grasses in open areas tend to have higher $\delta^{13}C$ values, while in forests the limited sunlight, high relative humidity, and the low $\delta^{13}C_{CO2}$ values related to the decaying organic matter in the soil lowers the $\delta^{13}C$ values of the undergrowth. These latter processes, in general, are collectively known as the canopy effect (van der Merwe and Medina, 1991; Bocherens et al., 1996; Cerling and Harris, 1999; Drucker et al., 2008).

Overall, the $\delta^{13}C$ values in tooth enamel depend on the isotopic composition of animal diet, which provides crucial information on climatic and environmental parameters (habitat) and the ecological traits (food preferences, trophic interactions) of animals (see Koch, 2007).

2.3. Stable oxygen isotope composition of enamel, environmental water and mean annual temperature

Oxygen isotope composition of the enamel of terrestrial

mammals depends on that of body water, which is in turn controlled by drinking and food water (e.g., Longinelli, 1984; Luz et al., 1984; Koch, 2007). Several variables affect herbivore tooth enamel $\delta^{18}O$ values, including drinking requirements (e.g., obligate, and non-obligate drinking animals), physiology (e.g., ruminant, non-ruminant species), the origin of ingested water (e.g., streams, ponds, rivers, lakes), and food type (e.g., fruits, leaves, grasses) (Ayliffe et al., 1992; Bryant and Froelich, 1995; Koch, 1998; Levin et al., 2006; Faith, 2018). Large, obligate drinking, non-ruminant herbivores are known to be good indicators of the environmental water O-isotope composition, while other species' water intake is mostly from food sources (non-obligate drinkers), which usually gives rise to higher $\delta^{18}O$ values for the body fluids. The $\delta^{18}O$ value of plants depends mostly on that of the water, the CO_2 oxygen isotope composition, as well as the relative ambient humidity and evaporation. Thus, the $\delta^{18}O$ values of animals consuming water-stressed plants also increase as a function of water deficit (Levin et al., 2006; Yann et al., 2013).

Oxygen isotopes of local precipitation ($\delta^{18}O_{ppt}$) are influenced by climatic and geographic variables such as temperature, latitude, altitude, continentality, humidity, precipitation amount, and moisture source (e.g., Dansgaard, 1964). Although it is not straightforward to tell apart the exact influence of each of these parameters, the annual average $\delta^{18}O_{ppt}$ values are largely controlled by an interplay of variations in temperature and the relative amounts of precipitation as these two are constrained by the other factors mentioned above. Hence, $\delta^{18}O_{ppt}$ values correlate in general most strongly with mean annual temperatures (MAT) over mid- and high-latitudes, in the absence of extremely low or high precipitation amounts (Dansgaard, 1964; Rozanski et al., 1993; Araguás-Araguás et al., 2000), where the so-called "amount-effects" dominate.

2.4. Climate and vegetation changes from the Zanclean to Early Pleistocene

In the Zanclean (5.3–3.6 Ma), which corresponds roughly to the MN14-MN15 Mammal biozones (Hilgen et al., 2012), simulated sea surface temperatures were 3–4 °C higher than today, with also a reduced latitudinal temperature gradient (Brierley et al., 2009; LaRiviere et al., 2012). Evidence from fossils analyzed from high latitudes confirms these model results: climate reconstructions based on beetle assemblages, tree growth rings, stable oxygen, carbon, and hydrogen isotopic compositions of larch trees indicate 10–15 °C higher than present-day temperatures in the North of Canada (Elias and Matthews, 2002; Ballantyne et al., 2006; Csank et al., 2011a,b). These reconstructions indicate that around 5 Ma the paleotemperatures were close to present-day temperatures and remarkable warming occurred between 5 and 4 Ma. In the Mediterranean and Western Europe, boreholes and terrestrial sediments provide continuous pollen sequences from that period (Suc et al., 1995; Fauquette et al., 1998). Climatic amplitude method (CAM) analyses demonstrate 1–5 °C warmer temperatures and 400–1000 mm higher than present precipitation at several sites of the peri-Mediterranean region (Suc et al., 1995; Fauquette et al., 1998, 1999, 2006; Bertini, 2001, 2010; Fauquette and Bertini, 2003; Jiménez-Moreno et al., 2010). Overall, the thermal gradients between Western Europe (France) and the Southern Mediterranean resembled those of the present-day, while the precipitation gradient was more accentuated. The mean annual precipitation (MAP) was higher than today between latitudes of 42 and 51°N (which corresponds to the study area at the investigated period) and it was similar or lower than modern values between about 30°N and 42°N latitudes (Sicily, Southern part of the Iberian Peninsula) (Fauquette et al., 1999, 2006; Bertini, 2010; Jiménez-Moreno et al., 2010; Combourieu-Nebout et al., 2015).

In the Piacenzian (3.6–2.8 Ma, ~ MN16 biozone) a succession of rapid climatic changes caused similarly rapid variations in the vegetation and the fauna (Agustí et al., 2001; Meyers and Hinnov, 2010; Rook and Martínez-Navarro, 2010; De Schepper et al., 2013, 2014; Woodard et al., 2014). The long-term trend was cooling and aridification with increased seasonality, which resulted in a strong decrease of subtropical trees and an increase of warm-temperate and cool-temperate trees as well as herbs in Western Europe (Suc et al., 1995). Following this trend, animals adapted to open habitats appeared in many regions and coexisted with the more archaic forest-dwelling species, (Rook and Martínez-Navarro, 2010; Petronio et al., 2011). A change in mean hypsodonty (crown height) of large mammalian herbivores further supports this pattern towards a more arid climate (Fortelius et al., 2002, 2006; Eronen and Rook, 2004). However, this cooling and aridification trend were not the same in different regions and changes reveal a high degree of spatial and temporal variability. After global cooling from 3.6 Ma and a short glaciation from 3.85 to 3.31 Ma, the "Mid-Piacenzian Warm Period" (MPWP) set in (Dowsett et al., 1996, 2010, 2013; Hill et al., 2011; Salzmann et al., 2011; Haywood et al., 2013; De Schepper et al., 2014). Over this period, western Europe was warmer and more humid than today, while the climate in the Southern Mediterranean was found to be warmer and similarly dry or drier than the modern climate (Fauquette et al., 1999; Salzmann et al., 2011). Model-data comparisons revealed some discrepancies regarding precipitation values. In Western Europe and the Northern Mediterranean area models underestimate wet conditions and overestimate precipitation amounts compared to pollen data over the Southern Mediterranean sector (Jost et al., 2009).

From 2.7 Ma (MN17 biozone) intensification of the Northern Hemisphere Glaciation (NHG) led to an irreversible climatic transformation in Europe, most probably linked to the final closure of the Panama Isthmus causing a major reorganization in the ocean-climate system (Haywood et al., 2002, 2013; Bartoli et al., 2005; Salzmann et al., 2011, 2013; De Schepper et al., 2013, 2014; Groeneveld et al., 2014). From this time on, the climate was dominated by glacial-interglacial cycles with a 41 ky periodicity. These fluctuations persisted until 0.9 Ma and strengthened with time (Meyers and Hinnov, 2010; Dowsett et al., 2013; Woodard et al., 2014; Salzmann et al., 2011, 2013; Haywood et al., 2013). Overall, the climate in longer-lasting interglacial periods was similar to that in the Pliocene, while MAT and MAP values were close to modern during the shorter glacial phases. In the glacial periods steppe-like vegetation spread at the expense of forests in the Mediterranean (e.g., Bertini, 2001, 2010; Combourieu-Nebout et al., 2015). Following the rapid changes in vegetation, a faunal turnover occurred with the spreading of large grazers and the disappearance of many forest-dwelling taxa (Palombo, 2007; Petronio et al., 2011).

3. Materials and methods

3.1. Studied fossils and chronology

Information about localities and investigated fossils included in this study can be seen in Table A1. Fig. 1 displays the geographic situation of the studied sites.

Some isotopic analyses were made on a new set of samples (n = 33) for this study, while the rest of the data were taken from works by Sánchez-Chillón et al. (1994), van Dam and Reichart (2009); Matson and Fox (2010); Domingo et al. (2013), Kovács et al. (2015, 2020), Johnson and Geary (2016) and Szabó et al. (2017). Most of the fossils belong to the families Rhinocerotidae (n = 66), Bovidae (n = 28), Gomphotheridae (n = 21), Equidae

Fig. 1. *Location of paleontological sites listed in Table A1 (the map shows the present-day locations). Inset map shows the Pliocene paleogeomorphology (from Popov et al., 2006).*

(n = 15) and Cervidae (n = 14), while only some samples are from other families (Table A1). To facilitate the evaluation of results in a temporal geological context, the samples were grouped into the Neogene Mammal (MN) biozones (Mein, 1975). Although the MN biozones represent biochronological relative ages, the boundaries of the MN biozones are defined by absolute ages, as the absolute ages of many European localities are known. In this study, the boundaries of the MN zones were used according to the geologic timescale of the International Commission on Stratigraphy (Hilgen et al., 2012), based on the works of De Bruijn et al. (1992), Oms et al. (1999), and Fejfar et al. (1998). Absolute ages of biozones, local faunas, and localities are listed in Table 1. Absolute ages are known for many of the investigated sites, while others are grouped into the MN biozones using biochronology.

3.1.1. Fossil samples analyzed for this study

Thirty-three samples out of the 149 included in this study were analyzed for stable carbon and oxygen isotope composition. Twenty-three samples are from the Massif Central region, located in the southeast of France, two samples are from Montpellier (southern France), and five samples are from Cebara (Bosnia and Herzegovina), and two samples are from Romania (Fig. 1).

The studied localities of Vialette, Seneze, and Chilhac from France have long been known to contain exceptionally well-preserved late Pliocene and early Pleistocene fossils. The localities represent maar environments and, in many cases, tephra and volcanic ash layers offered a good opportunity for radiometric dating. Mammal remains from Vialette have an absolute age of 3.14 ± 0.06 Ma (Lacombat et al., 2008). For the Chilhac locality, the ages have a range between 2.47 Ma and 1.8 Ma (Boivin et al., 2010). In Seneze, Roger et al. (2000) dated a tephra layer to 2.11 ± 0.01 Ma using $^{40}Ar/^{39}Ar$ method. The mammal fossils were most probably derived above this layer, so it was assumed that the age of the fossils is somewhat younger. Nomade et al. (2014) measured other tephra layers below and above the fossil-bearing layer, which gave comparable results, and thus the age of the fossils should be between 2.21 and 2.09 ± 0.02 Ma. The upper slope deposit analyzed by Paquette et al. (2021) is dated at 2.100 ± 0.029 Ma, consistent with an age younger than 2.104 ± 0.050 Ma for some of the recent fossil finds (Nomade et al., 2014). A second fossil layer dated between 2.176 ± 0.032 Ma and 2.132 ± 0.042 Ma by Nomade et al. (2014), also provides consistent ages within errors. The boundaries of some biozones seem to be somewhat different in the Nomade et al. (2014) study then used here. According to Nomade et al. (2014), the Seneze locality was the reference locality of MN18 in France. Nevertheless, the precise radiometric ages allow for integrating it into the MN17 biozone as used in this study. According to Paquette et al. (2021), zircons (U/Pb zircon ages) from both fossiliferous layers have statistically identical ages of 2.285 ± 0.046 Ma for Chilhac II and 2.262 ± 0.057 Ma for Chilhac III, in agreement with the 2.2 Ma age proposed by Bœuf (1997) based on the biochronological attribution to the MNQ17b biozone.

Most of the samples from the Massif Central belong to the rhinocerotid *Stephanorhinus etruscus* (n = 10), *Stephanorhinus megarhinus* (n = 4), while seven rhinoceros fossils were not identified at species/genus level (Table A1). Besides the rhinocerotid fossils, two samples from proboscidean were analyzed: one belonging to *Anancus arvernensis* and another to *Mammuthus meridionalis* (Table A1). The samples come from fossil teeth archived at the Laboratoire de Géologie de Lyon, Terre, Planètes, Environnement (LGL-TPE), University of Lyon (Lyon, France), Musée de paléontologie de Chilhac (France), and from the Natural History Museum Basel (Switzerland).

Five samples are from Cebara, which is a recently discovered site

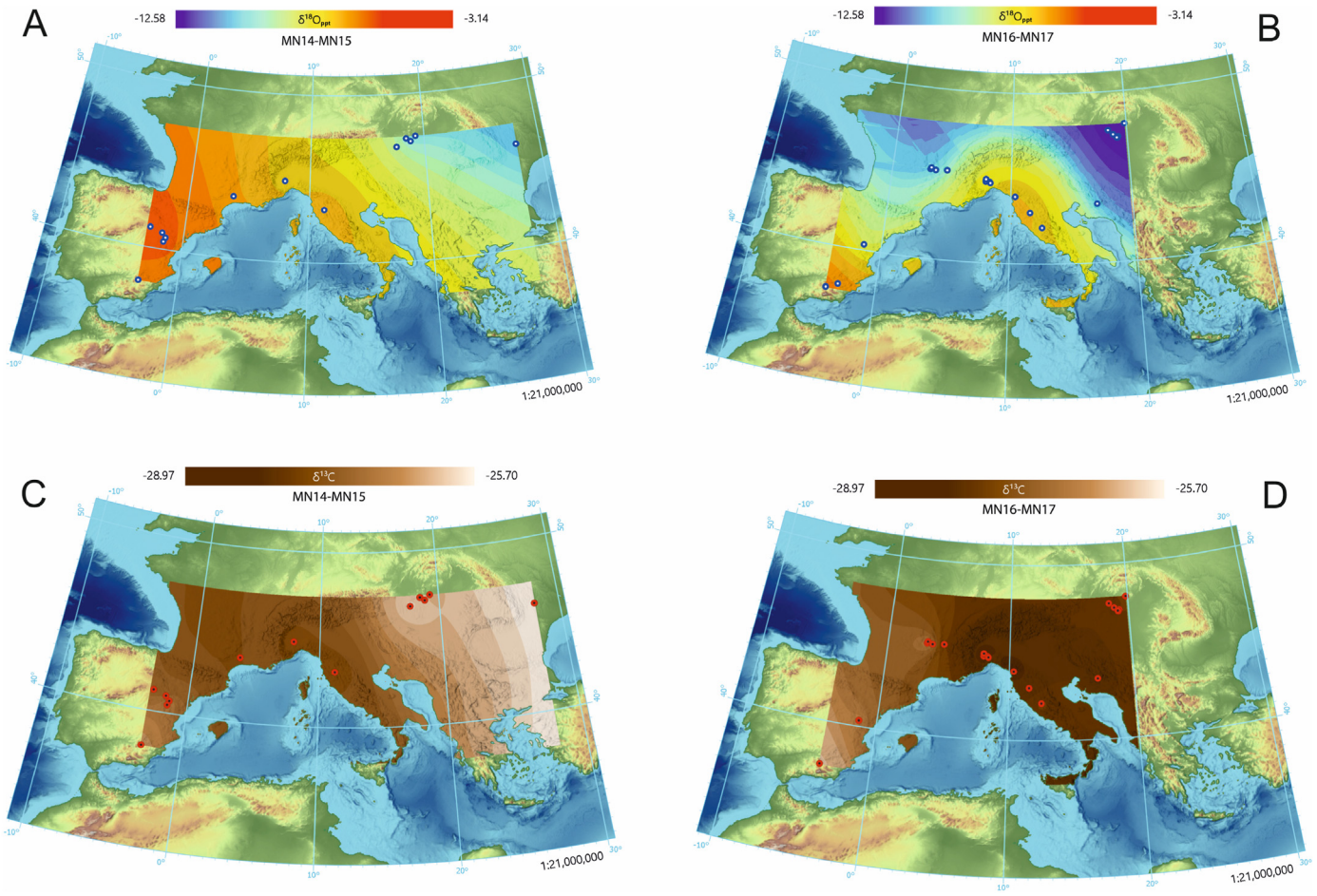

Fig. 2. *Color-interpolated maps of the calculated $\delta^{18}O_{ppt}$(‰, VSMOW) and calculated average $\delta^{13}C_{diet,meq}$(‰, VPDB) values in MN14-MN15 (A and C) and in MN16-17 (B and D) biozones. $\delta^{18}O_{ppt}$ scale was calculated using the equation of Kohn and Cerling (2002), $\delta^{13}C_{diet,meq}$ was calculated using the equations of Passey et al. (2005) and Kohn (2010).* A 5 Ma paleoDEM (Scotese and Wright, 2018) and rotation and geometry files for movement vectors (PaleoAtlas V3, Scotese, 2016) were used as major data sources for the reconstructed map. (For interpretation of the references to colour in this figure legend, the reader is referred to the Web version of this article.)

in the Dinaric karst in Bosnia and Herzegovina. The fossils most probably belong to *Anancus arvernensis* from the MN16 biozone (Table A1) (Mandić et al., 2013). All the material is stored in the Croatian Academy of Sciences and Arts (Zagreb, Croatia).

Samples from Romania are from the eastern parts of the country (Mânăstirea and Măluşteni), belong to *Stephanorhinus megarhinus* (n = 2) and are from the MN15a biozone (Table A1, Radulescu et al., 2003; Andreescu et al., 2013). Sampling was performed in the Laboratory of Palaeotheriology and Quaternary Geology of the Babeş-Bolyai University, (Cluj-Napoca, Romania) and the Museum of Oltenia, (MOC, Craiova, Romania).

3.2. Methods

The carbon and oxygen isotope results are reported in the common δ-notation, where $\delta_{sample} = [(R_{sample} - R_{standard})/R_{standard}]$ x1000, and $R = {}^{13}C/{}^{12}C$ or ${}^{18}O/{}^{16}O$. The carbon isotope compositions are expressed relative to the VPDB (Vienna Pee Dee Belemnite) standard, whereas the oxygen isotope composition is expressed relative to either the VPDB or the VSMOW (Vienna Standard Mean Ocean Water) standards.

Samples were taken with a Dremel® diamond-studded drill. Where it was possible the sample was taken over the whole enamel length from the crown to the root, but in some cases, enamel from tooth fragments was collected. Concerning the data from the literature, the sampling procedures were the same in most of the cases. Because of the complex process of tooth formation and mineralization, the samples likely represent an average isotope record of at least a few months in all sampling geometry stretching over a large enamel surface (Tafforeau et al., 2007; Metcalfe and Longstaffe, 2012). When results from several teeth are available from a location, the average isotopic result has been considered representative for the site. Most of the studies measured only tooth enamel, but Sánchez-Chillón et al. (1994) collected enamel and dentine together from their samples due to the small sample size. This has been taken into account in data interpretations.

Different studies used different pre-treatment and measurement methods (Table 2), which can lead to discrepancies in the final result. Some studies compare the effects of various sample treatments on the $\delta^{18}O$ and $\delta^{13}C$ values (Koch et al., 1997; Crowley and Wheatley, 2014; Pellegrini and Snoeck, 2016). However, these studies investigated the effects of pre-treatment only on the isotope compositions of the carbonate group. According to Koch et al. (1997), the different pre-cleaning steps did not significantly affect the structural carbonate carbon isotope values of enamel: the alteration of the $\delta^{13}C$ values was found to be within ±0.3‰. At the same time, the maximum deviation in $\delta^{18}O$ was +1‰ compared to untreated enamel. Crowley and Wheatley (2014) and Pellegrini and Snoeck (2016) observed larger deviations. They found that samples treated with acetic acid after organic removal pre-treatment

Table 1
Geological ages, MN biozones, faunal units, and local faunas.

approximate age (Ma)	epoch	age	MN biozones	faunal units and local faunas			references for MN boundaries
0.8	**Pleistocene**	**Calabrian**	**MN18/**		**Madonna della Strada, Pirro Nord, Val D'arno, Valle Berti,**		**Fejfar et al. (1998);**
0.9			**(MQ1)**	**Colle Curti, Fuensanta**	**Bugiulesti, Sant'Agata dei Goti, Barbinero di Mugello, Leffe,**		**faunal units:**
1				**Láchar**	**Veleni, Leu**		**Palombo, (2007)**
1.1							
1.2				**Barranco León**			
1.3				**Barranco del Paso**			
1.4				**Venta Micena**			
1.5				**Farneta**			
1.6				**Tasso, Cortes de Basa**			
1.7		**Gelasian**		**Olivola**			
1.8							
1.9			**MN17**		**Montefollonico, Becchi,**	**Chilhac, Nová Vieska, Castel**	**Oms et al. (1999)**
2				**La Puebla de Valverde**	**Pécel, Vecsés, Pilisvörösvár,**	**san Pietro, Incisa Belbo,**	
2.1				**Fuente Nueva 1**	**Pestszerntlőrinc**	**Stoina**	
2.2				**C. S. Giacomo, Seneze**			
2.3				**Cortio de Tapia**			
2.4				**Montopoli**			
2.5							
2.6				**Huélago**			
2.7	**Pliocene**	**Piacenzian**	**MN16b**			**Villafrancha d'Asti, Ferrere**	**Oms et al. (1999)**
2.8						**d'Asti, Castello d'Annone,**	
2.9						**Cebara, Cernatesti**	
3							
3.1				**Triversa, Vialette**			
3.2				**Hajnáčka**			
3.3			**MN16a**				**Oms et al. (1999)**
3.4							
3.5							
3.6		**Zanclean**	**MN15**		**Dusino san Paolo,**	**Szár 2, Huescar 3, Layna**	**De Bruijn et al.,**
3.7					**Százhalombatta, La Calera**		**(1992)**
3.8							
3.9							
4							
4.1				**Manastirea, Malusteni**			
4.2				**Gödöllő**			
4.3			**MN14**	**Pula, La Calera**		**Montarioso, Val di Pugna,**	**De Bruijn et al.,**
4.4				**Orrios**		**Montpellier, La Gloria 4**	**(1992)**
4.5							
4.6							

generally suffer from a variation of 0–1‰ in $\delta^{13}C$, while these offsets can reach 1.5‰ in $\delta^{18}O$. This implies that sample pretreatments can significantly alter the original isotopic compositions in some cases. However, because for carbonate the dissolved and/or reprecipitated structural and secondary carbonates introduce the largest variations, it is assumed that the pre-treatments have a much smaller impact on $\delta^{18}O$ values measured from the phosphate group (e.g., Kohn et al., 1999; Kohn and Cerling., 2002). Besides sample treatment, the various measurement methods performed by the different laboratories can also add some extra variations to the results, but for $\delta^{18}O_{PO4}$ the effects of the diverse pre-treatments and analyses can be small enough to have a negligible influence on interpretations. Results of studies obtaining $\delta^{18}O$ values only from the structural carbonates must be interpreted much more carefully. We assumed that the errors that may have been introduced by the different sample pre-treatment and measurement methods are usually smaller than the isotope variations reflecting environmental and climatic changes, but the possible effects have been taken into account in data interpretations.

3.2.1. Statistical analysis

To observe spatial and temporal differences, trends, and changes, the results were grouped into regions and biozones. Comparisons of mean values between regions and biozones were done using non-parametric Mann-Whitney tests. When more than two groups were compared, pairwise Mann-Whitney tests with Bonferroni corrections were performed. Statistical significance is set at $p < 0.05$.

3.2.2. Time averaging

Since the age estimates of samples can have large uncertainties, an unambiguous grouping of the samples into biozones was not always possible. For the spatial comparisons, all the samples from the Zanclean (MN14 and MN15 biozones) were examined together. Because most proxies and paleoclimate models indicate that the Zanclean (Lower Pliocene) climate was relatively stable for longer periods and the temperature fluctuations were smaller than in the Piacenzian (Upper Pliocene) and Pleistocene (Brierley et al., 2009; LaRiviere et al., 2012), it was assumed that the results of spatial comparisons refer to real spatial differences and are not the results of temporal climatic fluctuations over that period.

In contrast to the Zanclean, more intense, frequent climatic changes occurred during the Piacenzian and the Early Pleistocene. From around 3.3 to 3.0 Ma, a warmer and wetter than present period, the “Mid-Piacenzian Warm Period” (MPWP) occurred, while from 2.7 Ma onwards (MN17 biozone) the intensification of the Northern Hemisphere Glaciation (NHG) led to an alternation of glacial and interglacial periods (e.g. Dowsett et al., 1996, 2010, 2013; Haywood et al., 2002, 2013; Bartoli et al., 2005; Meyers and Hinnov, 2010; Hill et al., 2011; Salzmann et al., 2011, 2013; De Schepper et al., 2013, 2014; Groeneveld et al., 2014; Woodard et al., 2014). Averaging isotope data from long periods can mask the effects of

Table 2
Summary of the sample treatment methods and measurements.

literature	pre-treatment		phosphate separation	measurements, data management
	first step	second step		
this study, Kovács et al., (2015), 2020, Szabó et al., (2017);	NaOCl	acetic acid-Ca-acetate buffer	dissolved in HF, adding $AgNO_3$, precipitate as Ag_3PO_4; (Dettman et al., 2001; Kocsis et al., 2014)	$\delta^{18}O$ in PO4; (Vennemann et al., 2002) $\delta^{18}O$ and $\delta^{13}C$ in CO_3 (Spötl and Vennemann, 2003)
Johnson and Geary, 2016	NaOCl	acetic acid-Ca-acetate buffer	–	$\delta^{18}O$ and $\delta^{13}C$ in CO_3; ($\delta^{18}O_{PO4}$ were calculated from $\delta^{18}O_{CO3}$ values using the equation of Kovács et al. (2012) for equids
Van Dam&Reichart, 2009	NaOCl	acetic acid (0.1M)	–	$\delta^{18}O$ and $\delta^{13}C$ in CO_3; ($\delta^{18}O_{PO4}$ were calculated from $\delta^{18}O_{CO3}$ values using the equation of Kovács et al. (2012) for equids
Sánchez Chillón et al., 1994	H_2O_2, $KMnO_4$	–	$BiPO_4$ method, Tudge (1960); Longinelli (1966); Kolodny et al. (1983)	$\delta^{18}O$ in PO_4
Domingo et al., (2013)	H_2O_2	acetic acid-Ca-acetate buffer	dissolved in HNO_3; precipitate as Ag_3PO_4 (Bassett et al., 2007)	$\delta^{18}O$ in PO_4; $\delta^{18}O$ and $\delta^{13}C$ in CO_3
Matson and Fox, 2010	n.a.	n.a.	dissolved in HNO3 and precipitate as Ag_3PO_4 (Bassett et al., 2007)	$\delta^{18}O$ in PO_4

these rapid fluctuations but when interpreted carefully, the averaged data may provide useful information about the long-term trends.

According to the database, there are regions where samples from the MN16 and MN17 biozones can be compared, while in other regions there are larger age uncertainties, or the age of the locality is close to the MN16-MN17 boundary (for example Huélago, 2.6 Ma) and only the Zanclean (MN14-15) can be compared to the Piacenzian (MN16-17). The possible effects of time-averaging are discussed in more detail in the results and discussion sections below.

3.2.3. Testing diagenetic effects

For robust paleoclimatic and paleoenvironmental reconstructions, it is necessary to ensure that interpretations are based on unaltered, pristine stable isotopic data. The possible diagenetic effects were monitored with a proposed method by Iacumin et al. (1996), which is widely used in the literature (Bryant et al., 1996; Arppe and Karhu, 2006, 2010; Tütken et al., 2007; Pellegrini et al., 2011; Domingo et al., 2013). Studies of modern, non-altered enamel found that there is a constant offset between the $\delta^{18}O_{CO3}$ and $\delta^{18}O_{PO4}$ values of about 8.4–9.1‰ (Bryant et al., 1996; Iacumin et al., 1996; Martin et al., 2008; Pellegrini et al., 2011). Nevertheless, larger intra- and inter-tooth differences can also occur due to the complex process of enamel formation (e.g., Pellegrini et al., 2011; Trayler and Kohn, 2017). Hence, a $\delta^{18}O_{CO3} - \delta^{18}O_{PO4}$ offset of between 6.6 and 10.6‰ is likely to represent natural variations, while lower or higher offsets may indicate diagenetic alteration of the sample. All of the samples measured in this study and data collected from the literature have a $\delta^{18}O_{CO3} - \delta^{18}O_{PO4}$ offset between 6.6 and 10.6‰ (Table A1), implying that there is no pervasive diagenetic alteration of the samples.

3.2.4. $\delta^{13}C$ values, dietary behavior, and vegetation structure

Tooth enamel $\delta^{13}C$ values allowed us to reconstruct dietary composition and the modern $\delta^{13}C$ equivalent of the diet. This enables a more consistent interpretation of the results. The fractionation between diet and enamel depends on the body mass and physiology of the animal (Passey et al., 2005; Tejada-Lara et al., 2018). Passey et al. (2005) determined the dietary-bioapatite $\delta^{13}C$ enrichment ($\varepsilon^*_{diet\text{-}enamel}$) for different types of animals under laboratory conditions. The $\varepsilon^*_{diet\text{-}enamel}$ for non-ruminant large mammals is 13.3‰ based on pigs, while for ruminant mammals, it was found to be 14.6‰ based on cattle. Other authors give somewhat different fractionation factors based on wild animals. Koch (1998) found that $\varepsilon^*_{diet\text{-}enamel}$ is 12–14‰ for ungulates, while Cerling and Harris (1999) published a value of 14.1 ± 0.5‰ for non-ruminant mammals. The majority of measurements in this study are from Rhinocerotidae, but the database includes data from many different families, mostly from large and relatively large animals. Here we followed the work of Passey et al. (2005) and used a $\varepsilon^*_{diet\text{-}enamel}$ of 14.6‰ for the Bovidae and Cervidae families, while a $\varepsilon^*_{diet\text{-}enamel}$ of 13.3‰ was adopted for non-ruminant families.

The isotopic composition of atmospheric CO_2 changed through geological time, and it has an effect on $\delta^{13}C$ values of plants. To eliminate CO_2 effects, the modern equivalent of diet composition ($\delta^{13}C_{diet,meq}$) was calculated following the equations of Kohn (2010). Based on foraminifera data of Tipple et al. (2010) the $\delta^{13}C$ of atmospheric CO_2 was about −6.3‰ in the Pliocene, about −6.5‰ in the Pleistocene, and −8‰ for the present-day (Kohn, 2010). As suggested by Domingo et al. (2013), the calculated $\delta^{13}C_{diet,meq}$ values reflect different types of vegetation. Values above −20‰ indicate C_4 plant dominance in the vegetation, while values below this limit indicate different types of vegetation within a pure C_3 ecosystem. Values between −25 and −20‰ indicate open woodland - xeric grassland, between −30 and −25‰ imply woodland to woodland - mesic grassland, and values below −30‰ refer to a closed-canopy forest, as the main floral type.

Kohn (2010) proposed an equation to calculate the mean annual precipitation (MAP) from $\delta^{13}C_{diet,meq}$ values based on a compiled database integrating modern vegetation and precipitation data worldwide. There is a complex relationship between the type of vegetation and precipitation. Although the vegetation openness depends on MAP, other factors like temperature or the seasonal distribution of precipitation are equally important and, in some cases, the fauna itself can also affect their environment (Bakker et al., 2016; Doughty et al., 2016; Jeffers et al., 2018). Besides these complicating factors, there are some discrepancies between the results obtained by the precipitation equation and the vegetation reconstructions. The equation gives near-zero or negative values for precipitation when $\delta^{13}C$ values are higher than −25‰, while $\delta^{13}C$ values lower than −30‰ are likely biased by the canopy effect and could result in unrealistically high precipitation values. For $\delta^{13}C$ values between −30 and −25‰, both the vegetation estimation and calculated precipitation values are realistic. Because of these uncertainties, only the vegetation types and possible changes in vegetation were estimated, while the absolute MAP values or possible MAP changes were not calculated.

3.2.5. $\delta^{18}O_{PO4}$ values, isotope composition of precipitation, and mean annual temperature

The $\delta^{18}O$ of both carbonate and phosphate fractions of bioapatite in mammalian tooth enamel reflects the $\delta^{18}O$ value of body water, which in turn is controlled by oxygen uptake (inspired O_2 and water vapor, drinking water, dietary water, oxygen in food sources) and loss of oxygen (excretion, expired CO_2 and water vapor) during tooth development (Bryant and Froelich, 1995; Kohn, 1996). Particularly, there is a strong correlation between the $\delta^{18}O_{PO4}$ and $\delta^{18}O$ values of consumed water (environmental water, $\delta^{18}O_w$). Using established species-specific equations for modern fauna, $\delta^{18}O_w$ values can be calculated from bioapatite $\delta^{18}O_{PO4}$. Species-specific equations are sometimes based on small datasets and do not exist for all taxa. Nevertheless, because many species with different physiology show similar offsets from drinking water, general equations can also be used for calculating $\delta^{18}O_w$. In this study, the $\delta^{18}O_w$ values were estimated with two different general equations after Kohn and Cerling (2002; equation (1)) and Amiot et al. (2004; equation (2)) to get a possible range of environmental water compositions. Slopes of the two regressions are the same, so these give identical results if only the changes in $\delta^{18}O_w$ values are calculated.

$$\delta^{18}O_W = (\delta^{18}O_{PO4} - 23) / 0.90 \quad (1)$$

$$\delta^{18}O_w = 1.1128\ (\pm 0.0029)\ \delta^{18}O_{PO4} - 26.4414\ (\pm 0.0508) \quad (2)$$

The $\delta^{18}O_{PO4}$ values of some taxa track the $\delta^{18}O_w$ values closely whereas those of other taxa vary with aridity. For these evaporation sensitive (ES) taxa, the calculated $\delta^{18}O_w$ values can be higher than the real $\delta^{18}O_w$, particularly when the climate was arid, regardless of the equation used (general or species-specific) (Levin et al., 2006). In this study, the majority of the investigated taxa belong to evaporation insensitive (EI) or moderately sensitive families, and only some species from the *Cervidae* family fall into the evaporation sensitive category. These species, that also rely heavily on the water ingested through the consumed vegetation, may actually record higher calculated $\delta^{18}O_w$ results than the actual $\delta^{18}O_w$ from meteoric waters available in the area that they occupied.

The isotopic composition of environmental water ingested by EI animals is considered to be identical or very close to the $\delta^{18}O$ values of local precipitation ($\delta^{18}O_{ppt}$). However, it can deviate from $\delta^{18}O_{ppt}$ values under certain circumstances. For instance, under arid climate conditions, lake waters can have higher $\delta^{18}O$ values due to excess evaporation, while mostly glacier-fed rivers from a mountainous area can have markedly lower $\delta^{18}O$ values than the local $\delta^{18}O_{ppt}$.

Since there is a correlation between the $\delta^{18}O_{ppt}$ and mean annual temperature (MAT), the latter can be calculated (Dansgaard, 1964; Rozanski et al., 1993), assuming that the average $\delta^{18}O_{PO4}$ in teeth records meteoric water $\delta^{18}O_w$ and in turn, this value represents the average $\delta^{18}O_{ppt}$ of a given area. However, the correlation between $\delta^{18}O_{ppt}$ and MAT can be affected by factors including different moisture sources and air mass trajectories, latitude, altitude, continentality, and amount effects, and can change in time and space. When the correlation is weak, the type of dataset (local, regional, global, monthly, or annual averages) and the type of regression used are important in order to account for the overall variations as they could influence the paleoclimatic results and interpretations (e.g., Pryor et al., 2014; Skrzypek et al., 2016).

Overall, the absolute MAT calculations usually have large errors, and because of this, only the possible trends and changes in MAT (ΔMAT) were calculated here and not the absolute values. The slopes of four different regressions were used to estimate the possible range of MAT changes as inferred from $\delta^{18}O_{PO4}$ values, including two regional regression equations for Europe (Pryor et al., 2014; Skrzypek et al., 2016), and two global regression models (Dansgaard, 1964; Amiot et al., 2004) yielding a range of 1.41 °C/‰$_{\delta 18Oppt}$ to 2.04 °C/‰$_{\delta 18Oppt}$ gradients.

3.3. Mapping $\delta^{18}O_{ppt}$ and $\delta^{13}C_{diet,meq}$ values

Maps of the reconstructed stable isotope data were generated using ArcGIS Pro 2.7.2 (ESRI Inc., Redlands, CA, U.S.A.). Four major data sources were utilized to compile the stable isotope maps.

- 1 × 1 (approx. 111 km × 111 km), 5 Ma paleoDEM (Scotese and Wright, 2018) was used as a primary elevation source. This is a low-resolution digital elevation model (DEM) with temporally reconstructed elevation readings and spatial positions.
- The movement vectors were extracted for the 0 Ma → 5 Ma timeframe from the rotation and geometry files available in the PaleoAtlas V3 (Scotese, 2016). These vectors describe the displacement of a certain point in geographic space for the selected time window.
- Purely for visualization purposes, "The General Bathymetric Chart of the Oceans" (GEBCO) digital elevation model was utilized with a spatial resolution of 15′ × 15′ (approx. 460 m × 460 m; GEBCO Compilation Group, 2020) hosted by ESRI (ESRI, 2021).
- $\delta^{18}O$ and $\delta^{13}C$ values with their recent spatial locations.

With the help of the extracted movement vectors, the coordinates of the $\delta^{18}O$ and $\delta^{13}C$ values were shifted back to their assumed, original position for their estimated age (given in Ma). To improve the visual quality of the map's background the GEBCO DEM was also distorted by the movement vectors. However, the position of the pixels matches their historic position, the elevation values also still correspond to recent values. The 5 Ma paleoDEM raster was then merged with the distorted DEM by Empirical Bayesian Kriging Regression Prediction (Krivoruchko and Gribov, 2019), where the paleoDEM provided us the source dataset, and the distorted GEBCO DEM was the explanatory raster. The resulting DEM is a crude approximation yet visually fine-grained elevation raster. To interpolate the $\delta^{18}O$ values we used Empirical Bayesian Kriging with 100 simulations, a standard circular neighborhood with eight sectors. The coincident points were taken as average. The mean prediction error is −0.08162‰. The interpolated raster was clipped by the landmasses. For the $\delta^{13}C$ interpolation, the Empirical Bayesian Kriging was used too, with 100 simulations, smooth circular neighborhood with the smoothing factor of 0.2. The coincident points were taken as average. The mean prediction error is −0.05, which was also clipped by the landmasses.

4. Results

4.1. $\delta^{13}C$ values

The $\delta^{13}C$ values of the investigated fauna have a range from −16.3 to −8.2‰ (VPDB). In the MN14-15 biozones, the average $\delta^{13}C$ values of the four compared regions (Iberian Peninsula, Central, and North Italy, and Carpathian Basin) have a range from −14.1 to −11.4‰ (Fig. 3). Samples from the Iberian Peninsula show the highest mean $\delta^{13}C$ (−11.4 ± 0.6‰, n = 18), while the lowest values are from Central Italy (−14.1 ± 1.1‰, n = 7). Pairwise Mann-Whitney test with Bonferroni corrections indicate significant regional differences (Table 3), but there are also pairs of regions, where these are insignificant. Although the sample size in other regions is not sufficient to perform statistical tests, those data also add crucial information to the general picture. Two samples from

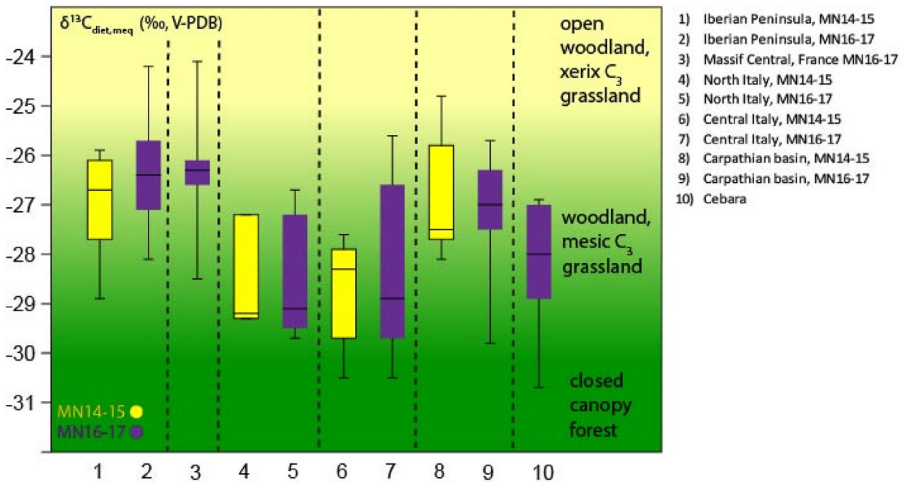

Fig. 3. $\delta^{13}C_{diet,meq}$ values in different regions and biozones. The modern equivalent vegetation was calculated using the equations of Kohn (2010). *The scale was calculated with Pliocene $\delta^{13}C$ values of atmospheric CO_2. Using a scale for the Early Pleistocene would shift the $\delta^{13}C_{diet,meq}$ values by +0.2‰.*

East Romania have higher $\delta^{13}C$ values (−11.3 ± 1.2‰, n = 2) compared to the mean values from other regions, while the two samples from Southern France have intermediate $\delta^{13}C$ values between Italy and the Iberian Peninsula (−12.6 ± 0.6‰, n = 2).

Stable isotope results of the MN16 and MN17 biozones can be compared for the South-East of France, northern Italy, and the Carpathian Basin. At the same time, for the Iberian Peninsula and Central Italy, only a mean value for the MN16-MN17 biozones can be obtained. A significant increase in $\delta^{13}C$ values is observed between the MN16 and MN17 biozones in North Italy (p = 0.02). In contrast, localities with precise radiometric ages in the Massif Central, France (Vialette - MN16; Seneze, Chilhac - MN17), and the Carpathian Basin (Table 4, Hajnáčka - MN16; Nová Vieska - MN17) also have similar $\delta^{13}C$ values in MN16 and MN17 biozones (p = 0.68 and p = 0.7, respectively). These almost constant values suggest that in these regions the mean values of the merged MN16-17 biozone may be representative for a longer period over a larger geographic extent.

Although averaging the results from MN16 and MN17 biozones can mask the possible temporal changes in some of the regions, the results of the merged MN16-17 biozone can be compared spatially. The average $\delta^{13}C$ values have a range from −13.9 to −10.6‰ (VPDB) and similarly to the MN14-15 biozone, pairwise Mann-Whitney test with Bonferroni corrections demonstrate several significant differences between the regions. Samples from the Iberian Peninsula have the highest $\delta^{13}C$ values (−10.6 ± 0.9‰, n = 24), while the lowest $\delta^{13}C$ values are from North Italy (−13.9 ± 1.1‰, n = 10).

Results from the MN14-15 and the MN16-17 biozones can be compared for four regions (the Iberian Peninsula, Northern, and Central Italy, Carpathian Basin, Fig. 2; 3, Table 4) and all of these regions are identical within their standard deviations.

4.2. $\delta^{18}O$ values

The phosphate $\delta^{18}O$ values relative to VSMOW have a range from 11.9 to 24.3‰ in the database. In the MN14-15 biozones, the mean $\delta^{18}O$ values have a range from 13.8 to 19.5‰ with the highest values from the Iberian Peninsula (19.5 ± 0.6‰, n = 21), and the lowest in Northern Italy (13.8 ± 0.8‰, n = 4). Comparing the four regions (Iberian Peninsula, North Italy, Central Italy, Carpathian Basin) the differences are clearly significant with the exceptions of those for Northern and Central Italy and Northern Italy and the Carpathian Basin (Table 3). Furthermore, two samples from Southern France have distinct $\delta^{18}O$ values, with an average being close to that of Central Italy. $\delta^{18}O$ values from East Romania are also similar to those from the Carpathian Basin (Fig. 4).

Just as for the $\delta^{13}C$ values, the differences in $\delta^{18}O$ values between the MN16 and MN17 biozones in Northern Italy are significant, while there is no significant trend for South-East France and the Carpathian Basin between these zones.

The mean $\delta^{18}O$ values have a range from 13.3 to 18.5‰ (VSMOW) in the merged MN16-17 biozone, with the highest values originating from the Iberian Peninsula (18.5 ± 0.9‰, n = 24) and the lowest from the Carpathian Basin (13.3 ± 1.6‰, n = 22). The spatial differences are significant between the Iberian Peninsula and all of the other regions, as well as between the Carpathian Basin and Central Italy or in comparison to the Massif Central region (Table 3. D). In contrast to the $\delta^{13}C$ values, notable temporal changes can be noted in the Carpathian Basin (p = 0.005) and Central Italy (p = 0.0006) between the MN4-15 and MN16-17 biozones (Fig. 2; 4, Table 4.).

5. Discussion

5.1. Vegetation distribution and its temporal changes from the Pliocene to Pleistocene and comparison with present-day vegetation

All the calculated $\delta^{13}C_{diet,meq}$ results are in the range typical of C_3 vegetation, implying that C_4 plants were a negligible or non-existent part of their diet. This is in agreement with other proxy data, which indicate that the contribution of C_4 plants to the total biomass was negligible in Europe over the Pliocene and early Pleistocene (Edwards et al., 2010). Provided that the vegetation is purely made up of C_3 plants, the $\delta^{13}C_{diet,meq}$ values can give further insight into the vegetation cover and climatic regime of the area, but species-specific habitat and dietary preferences may affect the general environmental context. Most of the species in our database are browsers and mixed feeders, which is supported by paleontological and ecological observations, tooth wear, and stable isotope compositions (e.g. Guérin, 1972, 1980; Mazza, 1988; Fortelius et al., 1993; Ji et al., 2002; Lacombat and Mörs, 2008; Janis, 2008; Kahlke and Kaiser, 2011; Domingo et al., 2013; Tütken et al., 2013; Rivals

Table 3
Results of the pairwise Mann-Whitney tests. Comparison of A) $\delta^{13}C_{diet,meq}$ values in MN14-15 biozones. B) $\delta^{18}O$ values in MN14-15 biozones, C) $\delta^{13}C_{diet,meq}$ values in MN16-MN17 biozones, D) $\delta^{18}O$ values in MN16-MN17 biozones in the different regions. The tables show the Bonferroni corrected p values. Significant differences are marked in yellow.

$\delta^{13}C$ values, MN14-MN15 biozones			
	Carpathian basin	Central Italy	North Italy
Central Italy	0.01881		
North Italy	0.4011	1	
Iberian Penninsula	1	0.001145	0.01931

A)

$\delta^{18}O$ values, MN14-MN15 biozones			
	Carpathian basin	Central Italy	North Italy
Central Italy	0.002699		
North Italy	1	0.06333	
Iberian Penninsula	0.00001889	0.03747	0.01248

B)

$\delta^{13}C$ values, MN16-MN17 biozones					
	Carpathian basin	Central Italy	North Italy	Central Massif	Iberian Penninsula
Central Italy	0.5501				
North Italy	0.2459	1			
Central Massif	0.4045	0.05207	0.001627		
Iberian Penninsula	0.000005272	0.001095	0.0001004	0.001695	
Cebara	1	1	1	0.06234	0.008688

C)

$\delta^{18}O$ values, MN16-MN17 biozones					
	Carpathian basin	Central Italy	North Italy	Central Massif	Iberian Penninsula
Central Italy	0.0004838				
North Italy	0.07079	0.1497			
Central Massif	0.000006003	0.07881	1		
Iberian Penninsula	0.0000001025	0.02563	0.0002662	0.000000697	
Cebara	0.05553	0.4791	1	1	0.02023

D)

et al., 2015; Saarinen and Lister, 2016; Haiduc et al., 2018).

Recent and Pleistocene rhinoceros species usually reveal diversity in their feeding habits (recent, Martin et al., 2008; Oloo et al., 1994; Pleistocene, Kahlke and Kaiser, 2011). The analyzed rhinoceros species in this study could be browsers and mixed feeders (Guérin, 1972, 1980; Mazza, 1988; Fortelius et al., 1993; Lacombat and Mörs, 2008). Similar dietary flexibility can also be observed in the case of recent (Cerling et al., 1999) and Pliocene proboscideans (Rivals et al., 2015; Saarinen and Lister, 2016; González-Guarda et al., 2018). Although *Equus* genus is traditionally considered grazers in open environments, there are many instances of *Equus* as browsers in forested environments in Pleistocene Europe (Rivals et al., 2015). Based on these data, it is assumed that the diet of most of the mixed feeders and many browsers could be adapted according to the availability in the habitat. Because of this, the overall assumption is that pooling the $\delta^{13}C$ values from different species into one average $\delta^{13}C$ can represent the average $\delta^{13}C$ value of the vegetation for each region and each biozone.

Most of the calculated $\delta^{13}C_{diet,meq}$ values in the database fall in the −30 and −25‰ range, only three values are below −30‰ and

Table 4
Temporal changes of $\delta^{13}C_{diet,meq}$ and $\delta^{18}O$ values in all of the studied regions.

significant temporal changes					
region	isotope	compared data sets	number of samples	p value (Mann-Whitney)	differences between the averages (‰)
Eastern France	$\delta^{18}O$	MN14 - MN16-17	2–21	0.042	−2.4
Northern Italy	$\delta^{13}C$	MN16 - MN17	5–4	0.02	2.1
Central Italy	$\delta^{18}O$	MN14 - MN16	7–9	0.0006	−1.4
Carpathian Basin	$\delta^{18}O$	MN15 - MN16-17	12–22	0.0006	−1
non significant temporal differences					
Iberian Penninsula	$\delta^{18}O$	MN14 - MN16-17	21–24	0.14	−1.1
Iberian Penninsula	$\delta^{13}C$	MN14 - MN16-17	18–24	0.14	0.5
Eastern France	$\delta^{18}O$	MN16 - MN17	8–14	0.09	0.4
Eastern France	$\delta^{13}C$	MN16 - MN17	8–14	0.68	0
Eastern France	$\delta^{13}C$	MN14 - MN16-17	2–21	0.09	1
Northern Italy	$\delta^{18}O$	MN14-15 - MN16-17	4–10	0.36	0.5
Northern Italy	$\delta^{13}C$	MN14-15 - MN16-17	4–10	0.94	−0.1
Northern Italy	$\delta^{18}O$	MN16 - MN17	5–4	0.1	−1.4
Central Italy	$\delta^{13}C$	MN14 - MN16-17	7–9	1	0.6
Carpathian Basin	$\delta^{13}C$	MN15 - MN16-17	11–22	0.7	−0.4
Carpathian Basin	$\delta^{18}O$	MN16 - MN17	6–10	0.7	1
Carpathian Basin	$\delta^{13}C$	MN16 - MN17	6–10	0.82	0.4

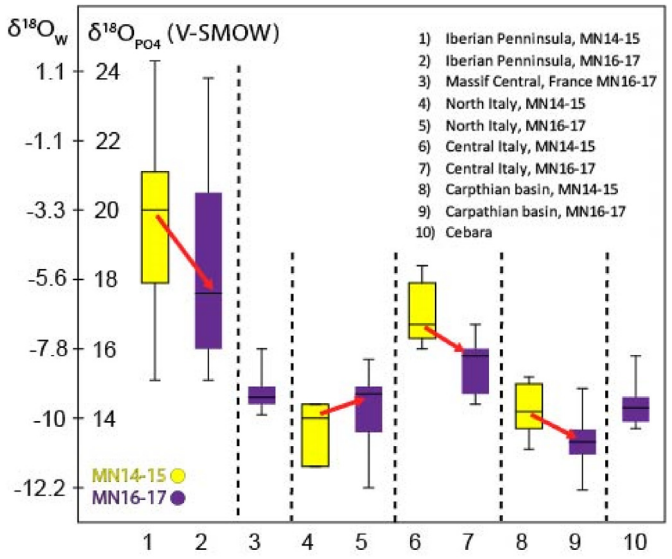

Fig. 4. *$\delta^{18}O_w$ (‰, VSMOW) values in different regions and biozones. The $\delta^{18}O_w$ scale was calculated using the equation of Kohn and Cerling (2002).*

six above −25‰. The mean values for each region and biozones are in the range between −30 and −25‰, indicating woodland to woodland - mesic grassland as a major flora type according to Domingo et al. (2013).

Overall, the spatial distribution of $\delta^{13}C_{diet,meq}$ values is in agreement with evidence retrieved from palynological records in the Zanclean (Table 5). For example, pollen assemblages from Northern Italy indicate vegetation dominated by hygrophilous, thermo-to mesothermic-forest taxa, typical of humid subtropical to warm-temperate climate (Bertini, 2001, 2010), while a dominance of herbaceous taxa, including many subdesertic species indicate dry and warm conditions for the Iberian Peninsula (Suc et al., 1995; Fauquette et al., 1998, 1999, Jiménez-Moreno et al., 2010). This contrast is reflected in the significantly lower $\delta^{13}C_{diet,meq}$ values (Table 3, Table 5) from North Italy, compared to values from the Iberian Peninsula.

In terms of absolute values, there are sometimes obvious discrepancies between indications of pollen data and $\delta^{13}C_{diet,meq}$ values. For Northern Italy, where both pollen data and models suggest closed forests with high MAP, the $\delta^{13}C_{diet,meq}$ values around −28.5‰ still indicate woodlands if the cut-off value of −30‰ is accepted for closed forests. In this sense, it is difficult to establish the limits between open forest and closed woodland conditions. Based on pollen sequences herbs can be present even in a forested environment in small proportions and the animals could live in swamp regions or along rivers, where more light could reach the undergrowth, resulting in higher $\delta^{13}C$ values of the vegetation. Besides, it is possible that the real cut-off $\delta^{13}C_{diet,meq}$ value of the closed-canopy forests can be somewhat higher than −30‰. The $\delta^{13}C$ values between −30 and −28‰ may indicate forest or more closed woodland, while values between −27 and −25‰ may refer to more open woodland or woodland/grassland environments.

In the MN16 and MN17 biozones the $\delta^{13}C_{diet,meq}$ values, and distributions are similar to the MN14-MN15 biozones (Fig. 2 C and D). Higher values from the Massif Central region (South-East France) and the Iberian Peninsula indicate more open woodland and/or lower MAP, while values from Central and Northern Italy and Cebara (Bosnia Herzegovina) suggest more closed woodland or forest and/or higher MAP. The results from the Carpathian Basin are intermediate between these two groups (Fig. 3). The overall distribution agrees with the information provided by palynology and other paleontological data (Table 5), but as described above, the boundary between forest and woodland vegetation is difficult to establish based on $\delta^{13}C_{diet,meq}$ values.

The temporal differences between MN14–15 and MN16-17 are usually lower than the spatial ones between the various regions, which overall indicate a relative homogeneity and low compositional variability of the vegetation over time through the Pliocene and Early Pleistocene. However, smaller-scale changes in $\delta^{13}C_{diet,meq}$ values may indicate compositional shifts in vegetation in some regions. In the Iberian Peninsula the change from MN14-15 to MN16-17 biozones is not significant ($p = 0.14$, Table 4), but the average $\delta^{13}C_{diet,meq}$ value increases by about 0.5‰, which potentially points towards a somewhat more arid climate in that region (Fig. 4.). In Central and Northern Italy, mean $\delta^{13}C$ values in the MN16-17 biozone are close to those in the MN14-15 (Fig. 3; Table 5), but in Northern Italy, where the MN16 and MN17 biozones can be studied separately, the values in the MN17 biozone are significantly higher ($p = 0.02$, Table 4) than in the MN16 biozone. This suggests that in Italy the vegetation did not profoundly change over the Zanclean and Piacenzian, while larger transformations occurred at and around the Pliocene – Pleistocene boundary. The Massif

Table 5
Comparison of pollen indications, paleontological proxies and $\delta^{13}C_{diet,meq}$ values. Cited literature: 1) Suc et al., (1995); 2) Fauquette et al., (1998), 3) Fauquette et al., (1999); 4) Jiménez-Moreno et al., 2010; 5) Bertini, (2001); 6) Bertini, (2010); 7) Nomade et al., (2014); 8) Cirilli et al., (2021); 9) Guérin et al., 2004; 10) Lacombat et al., (2008); 11) Pontini and Bertini, (2000); 12) Combourieu-Nebout et al., (2015); 13) Martinetto et al., (2017); 14) Hably and Kvaček, (1998).

	MN14-15		MN16-17		recent
	pollen and other paleontological information	avg. δ^{13}Cdiet,meq	pollen and other paleontological information	avg. δ^{13}Cdiet,meq	
Iberian Peninsula	Garraf 1: coastal forest, dominance of mega-mesothermic trees, Taxodium-type plants, swamp conditions. Tarragona: predominance of herbs, mainly Asteraceae and Poaceae (1; 2; 3; 4) including subdesertic taxa, dry and warm conditions (2; 4). South Spain, Andalucía, G1 core: similar to Tarragona, but trees are also well represented due to a nearby relief (1; 2; 4)	−26.9‰	Garraf 1; 3.4 Ma: cooling event, strong decrease of mega-mesothermic trees, increase in herb pollen. 3.1−3.0 Ma: Weak warming, final occurrence of subtropical taxa in high abundances (1; 2; 3; 4). From 2.7 Ma: reduced extent of coastal forest, increase of Artemisia taxa, decrease of arboreal taxa (1; 2; 3; 4). Steppe- and forest-dominated periods alternated rapidly (2), the long-term trend was aridification.	−26.4‰	Mediterranean sclerophyllous forests and shrubs
Massif Central, France	–	–	Vialette, 3.14Ma: First appearance of genus Equus (10). From 2.6 Ma to 2.4 Ma, MN17: Rapid spread of grazers (7,8). Saint Vallier, ~2 Ma, MN17: mosaic steppe punctuated by open woodland, based on the mammalian community (9).	MN16: 26.3‰ MN17: 26.3‰ MN16-17: 26.3‰	beech forest
North Italy	Stirone and other sites: vegetation dominated by hygrophilous, thermo- to mesothermic-forest taxa, humid subtropical to warm-temperate climate (5; 6).	−28.4‰	a cooler type of forest than in the Pliocene during glacial periods (5; 6; 11; 12)	MN16: 29.4‰ MN17: 27.2‰ MN16-17: 28.5‰	thermophilus mixed deciduous broad-leaved forest
Central Italy	Southern Italy, Sicily: deciduous forest taxa were subordinate to the non-arboreal associations, presence of some subdesertic plants, arid climate. (6)	−28.8‰	from 2.7 Ma: steppe conditions during glacial periods in Southern and partly in Central Italy (5; 6; 11; 12). Central-Southern Italy: locally warmer and wetter climate, the thermophile and humidity-requiring woody plant taxa persisted longer (until 1.8 Ma) than in many other regions (13)	MN16-17: 28.5‰	thermophilus mixed deciduous broad-leaved forest
Carpathian Basin	Pula locality (4.25 ± 0.17 Ma): warm temperate forest vegetation, but small-leaved plant species (e.g., Querqus kubinyii), 600−1200 mm MAP and a seasonal dry period (14).	−26.8‰	–	MN16: 27.0‰ MN17: 26.7‰ MN16-17: 27.2‰	thermophilus mixed deciduous broad-leaved forest, steppe alternating with oak forests in the South-Eastern part
Cebara, Bosnia-Hercogovina	–	–	–	−28.3‰	thermophilus mixed deciduous broad-leaved forest

Central (France) is undersampled in the MN14-15 biozones, but the MN16 and MN17 biozones can be studied separately due to the existence of localities with precise radiometric ages. The $\delta^{13}C$ values are relatively high and are almost the same in both the MN16 and MN17 biozones (Table 4). The lack of change is partly in disagreement with the information obtained from faunal assemblages, showing a rapid spread of grazers from 2.6 Ma to 2.4 Ma (MN17, Nomade et al., 2014; Cirilli et al., 2021). In the Carpathian Basin, there is no clear long-term trend in the $\delta^{13}C_{diet,meq}$ values. Although the average $\delta^{13}C_{diet,meq}$ value is 1‰ lower in the MN16-17 biozones, compared to the MN15 biozone, this change does not prove to be significant ($p = 0.7$, Table 4), and similarly to South-Eastern France, significant change is not observed in the comparison of the MN16 and MN17 biozones ($p = 0.82$, Table 4).

The reconstructed vegetation for the Pliocene and Pleistocene can be compared with the modern-day vegetation in the studied regions. In most of Europe, the recent natural vegetation is profoundly altered by agriculture, but the natural vegetation has been reconstructed in a comprehensive study (Bohn et al., 2000). As discussed above, it is difficult to separate closed woodland and open canopy forest based on the $\delta^{13}C$ values, but these can still be indicative of vegetation openness and/or aridity. The reconstructed woodland and/or mesic grassland with more closed vegetation in North and Central Italy and more open vegetation in the Iberian Peninsula and partly in the Carpathian Basin for the Pliocene and Early Pleistocene seems to be similar to the present-day vegetation. The largest difference between the reconstructed and recent vegetation is found to be in the Massif Central region, where modern vegetation would be mainly beech forest, and because of the diverse topography, thermophilus mixed deciduous broad-leaved forest and pine forests would also be present. In contrast, for the MN16-MN17 biozones, the relatively high $\delta^{13}C$ values are similar to those from the Iberian Peninsula, indicating relatively open woodlands and/or low MAP. The reconstructed mosaic steppe and open woodland vegetation based on the mammalian community (Guérin et al., 2004) agree with the $\delta^{13}C$ results in the MN17 biozone. The topography of the Massif Central area can have a strong effect on the vegetation, but it is unlikely to explain all the differences. The area has a complex climate as it is partly under the influence of Mediterranean, Atlantic, and continental climates. It is conceivable that in areas like this even a smaller scale change in global or regional climate or shifts in air mass trajectories are able to alter the local climate significantly.

5.2. Patterns and temporal changes of $\delta^{18}O_{ppt}$ from the Pliocene to Pleistocene and comparison with present-day values

The majority of investigated taxa belong to evaporation insensitive (EI) or moderately sensitive families and only some samples of evaporation sensitive (ES) taxa are included. The highest $\delta^{18}O_{PO4}$ values are from the ES cervids and moderately sensitive bovids with the highest value from a *Gazella borbonica* sample from Layna (Tajo Basin, Spain). The calculated $\delta^{18}O_{ppt}$ values from that sample have a range between 0.6 and 1.4‰ depending on the equation used (Kohn and Cerling, 2002; Amiot et al., 2004). The positive $\delta^{18}O_{ppt}$ value seems to be an overestimation because the $\delta^{18}O$ value of the ocean was close to 0‰ over the Pliocene and the $\delta^{18}O$ values in precipitation rarely exceed 0‰ due to the isotopic fractionations during evaporation and condensation. It seems likely that in some cases aridity and physiological adaptation of the animals could result in higher tooth enamel $\delta^{18}O_{PO4}$ values, and consequently, the real $\delta^{18}O_{ppt}$ could be lower than the calculated ones. Alternatively, secondary evaporation of surface waters or precipitation may lead to $\delta^{18}O_{ppt}$ values higher than 0‰ as is commonly noted today in central-eastern Africa. This effect must be considered for samples obtained from the Iberian Peninsula, where all the ES and moderately sensitive taxa are present. Together with this the mean value, which includes all the results from the ES, moderately sensitive, and EI taxa, can still be close to the $\delta^{18}O_{ppt}$ value of the area.

In the MN14-15 biozones, the calculated mean annual $\delta^{18}O_{ppt}$ values are similar to present-day values in three of the four study regions (Table 6), while in Northern Italy these values are lower than those of the present-day (−10.7‰ vs −6 to −8‰).

It is suggested that a local effect, namely the surface waters of Alpine catchments with low $\delta^{18}O_{ppt}$ values may have lowered the $\delta^{18}O_{ppt}$ values in that region (Szabó et al., 2017). Thus, MAT differences were not calculated using these values. Nevertheless, in the other three regions MAT estimations can be informative. In the Iberian Peninsula, the samples from various species, including ES and moderately evaporation sensitive taxa, are also from different regions with complex topography, as well as being regions that are under the influence of Atlantic and Mediterranean marine-derived air masses, but with likely local re-evaporation from Central European and African continental areas influencing the moisture in the air masses (e.g., Araguas-Araguas and Diaz Teijeiro, 2005; Hatvani et al., 2020). Such complexities may explain the higher variability of $\delta^{18}O_{ppt}$ values compared to that measured in other regions (Fig. 4). Overall, the higher average $\delta^{18}O_{ppt}$ value compared to Central Italy or the Carpathian Basin appears to be realistic, even though the 2.9‰ difference compared to Central Italy is higher than that for present-day conditions (about 1–2‰ only, Araguás-Araguás and Díaz Teijeiro, 2005; Giustini et al., 2016).

Few samples are available from other regions. The two fossils from Southern France have distinct $\delta^{18}O$ values with an average close to those from Central Italy. Because these samples are from a locality near the Mediterranean (sampled close to Montpellier), it is likely that the $\delta^{18}O_{ppt}$ values from localities further from the sea would be somewhat lower. The average value of the two samples from Romania (14.7‰) resembles the average value of the Carpathian Basin (14.3‰), which may indicate a similar MAT. Recent MATs are almost the same in the two regions, with a higher degree of continentality in South-Eastern Romania (Croitoru et al., 2013).

Overall, the spatial distribution of the $\delta^{18}O_{ppt}$ is similar to that for the present-day conditions in regions compared in this study, with local exceptions that may well have experienced changes in the local conditions for the precipitation.

In the MN16-17 biozones, the $\delta^{18}O_{ppt}$ variations between the regions are similar to those of the MN14-15 biozones (Table 3). The average $\delta^{18}O_{ppt}$ is the lowest in the Carpathian Basin, the highest in the Iberian Peninsula, while values from South-Eastern France and Central Italy are intermediate between these. Comparing the South-Eastern France region with the Carpathian Basin, the 1.4‰ higher $\delta^{18}O_{PO4}$ values in the former may indicate 1.5‰ higher $\delta^{18}O_{ppt}$ values and 2.2–3.8 °C higher MAT, provided that the higher $\delta^{18}O_{ppt}$ values can exclusively be explained by temperature changes. This difference is similar to the present-day differences between the two regions (Massif Central, France: $\delta^{18}O_{ppt}$: −6 to −8‰, MAT 13–15 °C, Carpathian Basin: $\delta^{18}O_{ppt}$: −8‰, MAT 10–11 °C). However, estimating the MAT from $\delta^{18}O_{ppt}$ values is exceptionally difficult for the Massif Central region. In contrast to many other regions in Europe, there is no correlation between the MAT and $\delta^{18}O_{ppt}$ values in that area as demonstrated by data from a nearby IAEA GNIP station (International Atomic Energy Agency, Global Network of Isotopes in Precipitation, Orgnac/Chauvet cave, Genty et al., 2014). At that station, the $\delta^{18}O_{ppt}$ values vary independently of MAT over the period 2001 to 2011, regardless of the year, month, or the $\delta^{18}O_{ppt}$ value weighted by rainfall amount. The reason for the lack of correlation can be the effect of being at a cross-section between different Mediterranean and Atlantic air masses, and the uneven yearly distribution of precipitation due to important rain-out effects during winter and summer storms, which are common in the region and, similarly to monsoonal regions would have the “amount” effect as a dominant factor of the variations in $\delta^{18}O_{ppt}$ values.

In the Iberian Peninsula, the calculated average $\delta^{18}O_{ppt}$ value is 3.3‰ higher than in Central Italy, and similarly to the MN14-15 biozones, $\delta^{18}O$ variability is also higher than in other regions. As for the MN14-15 biozones, the higher than present-day difference can be a slight overestimate due to the presence of the ES and moderately evaporation-sensitive taxa.

Regarding the temporal changes, the calculated $\delta^{18}O_{ppt}$ values are lower in the MN16-17 than in the MN14-15 biozones (Fig. 4) for most of the regions. The decrease is 1.5‰ in Central Italy and 1.1‰ in the Carpathian Basin, implying a 2–3 °C decrease of MAT in Central Italy and 1.5–2 °C MAT decrease in the Carpathian Basin. This change is not significant in the Iberian Peninsula ($p = 0.14$,

Table 6
Calculated average $\delta^{18}O_{ppt}$ values and comparison with the present-day $\delta^{18}O_{ppt}$ values. The possible range of $\delta^{18}O_{ppt}$ values was calculated using two different general equations of Kohn and Cerling (2002) and Amiot et al. (2004). References: 1: Araguás-Araguás and Díaz Teijeiro (2005); 2: Genty et al. (2014); 3: Longinelli and Selmo (2003); 4: Giustini et al. (2016); 5: Vodila et al. (2011), 6: Holko et al. (2012); Horvatinčić et al. (2005).

	MN14-MN15				MN16-MN17				present day	references
	n	avg. $\delta^{18}O_{PO4}$	std.	calculated $\delta^{18}O_{ppt}$	n	avg. $\delta^{18}O_{PO4}$	std	calculated $\delta^{18}O_{ppt}$	$\delta^{18}O_{ppt}$	
Iberian Penninsula	18	19.5	2.2	−4.3 ± 2.9	24	18.5	2.5	−5.4 ± 3.2	−4–-7	1
Central Massif, France					21	14.7	0.5	−9.7 ± 1	−6–-8	2
North Italy	4	13.8	0.8	−10.7 ± 1.3	10	14.3	1.1	−10.1 ± 1.7	−6–-8	3, 4
Central Italy	7	16.9	0.9	−7.2 ± 1.4	9	15.6	0.7	−8.7 ± 1.2	−5–-8	3, 4
Carpathian Basin	12	14.3	0.7	−10.1 ± 1.2	22	13.3	0.7	−11.2 ± 1.2	−8–-10	5, 6
Cebara					5	14.5	0.8	−9.9 ± 1.3	−5–-9	7

Table 4), but the decrease of the mean $\delta^{18}O_{ppt}$ value is 1.1‰. The shift in the average $\delta^{18}O$ value is 2.4‰ in Eastern France, but no $\delta^{18}O_{ppt}$ and MAT changes were calculated for this region, as only two samples are available from the MN14-15 biozones. The only exception to the decreasing trend is Northern Italy, where the mean values show limited variability in the MN14–15 and MN16-17 biozones. In this region, the MN16 and MN17 biozones can also be compared, and a significant difference was found between these two biozones. As described above, we assume that local factors could have a strong effect on the $\delta^{18}O$ values in this region and these may not have followed the changes in $\delta^{18}O_{ppt}$, hence MAT changes were therefore not calculated.

In the other two regions, where the fossils of MN16 and MN17 biozones allowed for a comparison (South-Eastern France and the Carpathian Basin) the results are identical in the two biozones. This contradicts other proxy and model results, which reveal a cooling trend from 2.7 Ma onwards (Dowsett et al., 1996, 2010, 2013, among others). Causes that would unambiguously explain these differences are unknown to us, but if the samples from these two regions are from an interglacial period this could explain the similar MN16 and MN17 climates.

The calculated $\delta^{18}O_{ppt}$ values can be compared with present-day values in each region (Table 6). In the Iberian Peninsula, calculated $\delta^{18}O_{ppt}$ are in the range of modern precipitation both in the MN14–15 and MN16-17 biozones. In the Massif Central, France the calculated $\delta^{18}O_{ppt}$ values vary between −9 and −10‰ in the MN16 and MN17 biozones, while recent values range from −6 to −8‰. Since there is no correlation between $\delta^{18}O_{ppt}$ and MAT in that region at present, (see more details in the previous section), the difference does not necessarily reflect a change in MAT. If it is assumed that these $\delta^{18}O_{ppt}$ deviations reflect solely MAT differences, the global and European $\delta^{18}O_{ppt}$ – MAT equations (Dansgaard, 1964; Amiot et al., 2004; Pryor et al., 2014; Skrzypek et al., 2016) would result in a 3–7.5 °C lower than present-day MAT. This would be in contrast to climate model results for the Piacenzian (e.g., Dowsett et al., 1996, 2010, 2013) and is considered unrealistic. Factors other than MAT may have caused the change in $\delta^{18}O_{ppt}$ values. The variation in the proportion of air masses of Atlantic, continental, and Mediterranean origins affecting the region or the amount and annual distribution of precipitation over geologic time may explain such $\delta^{18}O_{ppt}$ values. This assumed difference compared to the present-day climate is also supported by the $\delta^{13}C$ values. The $\delta^{13}C$ values indicate more open vegetation than characteristic for the present-day and/or more arid climate and among the studied regions only the Massif Central area shows a marked shift compared to the present day.

In Central Italy, the recent annual average $\delta^{18}O_{ppt}$ values are between −8 and −5‰, depending on the topography and the distance from the sea (Longinelli and Selmo, 2003; Giustini et al., 2016). The calculated average $\delta^{18}O_{ppt}$ for the MN14-15 biozones are close to present-day values, while for the MN16-17 biozones they are lower. In the Carpathian Basin, the recent $\delta^{18}O_{ppt}$ values have a range between −9 and −8‰ (Vodila et al., 2011; Holko et al., 2012). The calculated $\delta^{18}O_{ppt}$ value for the MN14-15 is identical to the present-day values, while in MN16-17 it is lower. The calculated $\delta^{18}O_{ppt}$ value for the MN16-17 biozones is also lower than the present-day values in Cebara.

Because other proxies and models give higher than present-day MAT in the Early Pliocene and usually similar or higher than present-day MAT in Late Pliocene and during the glacial-interglacial cycles in the Early Pleistocene, the calculated $\delta^{18}O_{ppt}$ values are overall lower than expected. In Northern Italy and the Massif Central, France, where the differences are the highest, possible regional effects may control local water $\delta^{18}O$ values, leading to lower $\delta^{18}O$ values in the teeth, but in other regions, the situation is more complicated.

In summary, the absolute $\delta^{18}O_{ppt}$ values are somewhat lower than expected when compared with present-day $\delta^{18}O_{ppt}$ values, but most of the changes and differences in $\delta^{18}O_{ppt}$ values in time and space seem to be realistic for the Pliocene and Early Pleistocene.

6. Conclusions

Carbon and oxygen stable isotope compositions of tooth enamel from large mammals were reviewed from the literature and complemented with new measurements of this study in order to evaluate regional changes in climate and vegetation during the Pliocene and Early Pleistocene. Based on the $\delta^{13}C$ values, the reconstructed vegetation can be characterized as woodland to woodland – mesic grassland in all of the investigated regions and biozones in a pure C_3 ecosystem. Spatial and temporal changes in the $\delta^{13}C$ values follow the changes in openness of the vegetation and/or in aridity.

The $\delta^{13}C$ values and their spatial distribution is similar in the Early Pliocene and the Late Pliocene to Early Pleistocene, implying that the changes in the vegetative cover that were induced by climatic change in each region were smaller than the spatial differences between the studied regions. The vegetation was more closed in Central and Northern Italy and Cebara and more open in the Iberian Peninsula, in the Massif Central regions, in the Carpathian Basin, as well as in Eastern Romania. The reconstructed distribution of the vegetation and/or the amount of precipitation for most of the regions was comparable that of today for most of the regions investigated so far. An exception is given by the Massif Central region, where a more pronounced difference is noted. It is assumed that because this area is partly under the influence of Mediterranean, Atlantic, and continental climates, even smaller-scale changes in global or regional climate or shifts in the direction of air masses can affect the local climate. The $\delta^{18}O$ values also support this assumption: the difference between the reconstructed and present-day $\delta^{18}O_{ppt}$ values is also the highest for this particular region.

The spatial distributions of the calculated $\delta^{18}O_{ppt}$ values are broadly similar for Early Pliocene and Late Pliocene to Early Pleistocene. Three regions (Iberian Peninsula, Central Italy, and Carpathian Basin) from where abundant fossils were available, indicate a 1–1.5‰ decrease in $\delta^{18}O_{ppt}$ values between the MN14–15 and MN16-17 biozones, potentially representing a 1.5–3 °C decrease in MAT. This long-term cooling trend from the Early Pliocene to the Early Pleistocene is in agreement with the results of other proxies and climate models. In contrast, from three regions (Massif Central, North Italy, Carpathian Basin), for which the MN16 and MN17 biozones (Pliocene – Pleistocene boundary) can be compared, the $\delta^{18}O_{ppt}$ values suggest a decrease only in Northern Italy. The constant $\delta^{18}O_{ppt}$ values through the Pliocene – Pleistocene boundary in the Massif Central and the Carpathian Basin contradict other proxies. However, samples from the MN17 biozone may be from interglacial periods when the climate resembled that in the Pliocene.

The calculated $\delta^{18}O_{ppt}$ values are in the range of present-day $\delta^{18}O_{ppt}$ values in MN14-15 biozones for most of the regions, while the values for the MN16-17 biozones are usually lower. Because other proxies indicate warmer than the present-day climate in the Early Pliocene and similar to the present-day climate in Late Pliocene and Early Pleistocene, the values are overall lower than expected. In some regions, such as in northern Italy, the most likely explanation for the lower values is the effect of low $\delta^{18}O$ values of river waters from high mountainous areas. However, because multiple factors exert control on the $\delta^{18}O_{PO4}$ values in mammal

teeth and the $\delta^{18}O_{ppt}$ values calculated for each region are also prone to complexities due to local geographic effects as well as errors in the parameters used for the calculations, the discrepancies cannot so far be fully resolved. Overall, the interpretations based on the $\delta^{18}O_{PO4}$ differences and related to similar differences in the $\delta^{18}O_{ppt}$ values, are more robust than interpretations based on the absolute values calculated for the precipitation.

Author contributions

All authors made substantial contributions to the manuscript and writing/editing the paper. Péter Szabó served as PI for the project, drafted most of the paper, and prepared all the figures together with Ákos Halmai. János Kovács, Torsten Vennemann, László Kocsis and Laura Domingo served as co-PIs for the project wrote the paper and contributed to its editing. Gábor Újvári and Vlad Codrea were involved in the project design and edited the manuscript contributing to the interpretations. Ákos Halmai and Ervin Pirkhoffer served as GIS experts and contributed to the mapping presented in Fig. 2. All the authors participated in the revising of the manuscript since its initial review by the journal.

Declaration of competing interest

The authors declare that they have no known competing financial interests or personal relationships that could have appeared to influence the work reported in this paper.

Acknowledgments

The research has been generously funded by the Swiss SCIEX program Nr. 13.083 and the Hungarian NRDIO K120213 and 2020–4.1.1-TKP2020 grants. The authors are grateful to Frederic Lacombat, (formerly Paleontology Museum of Chilhac) Loïc Costeur (Natural History Museum Basel), Robert Emmanuel (Laboratory of Geology of Lyon: Earth, Planets, and Environments), Aurelian Popescu (Museum of Oltenia), and Oleg Mandic (Natural History Museum Vienna) for supplying the fossil materials. L. Domingo acknowledges the support of project PGC 2018-094955-A-I00 of the Spanish *Ministerio de Ciencia, Innovación y Universidades* and research group UCM 910607 on Evolution of Cenozoic Mammals and Continental Palaeoenvironments. Two anonymous reviewers are thanked for their useful and constructive comments and suggestions. We are also grateful to Dr. Miryam Bar-Matthews for her editorial handling.

Appendix A. Supplementary data

Supplementary data to this article can be found online at https://doi.org/10.1016/j.quascirev.2022.107572.

References

Agustí, J., Cabrera, L., Garcés, M., Krijgsman, W., Oms, O., Parés, J.M., 2001. A calibrated mammal scale for the Neogene of Western Europe. State of the art. Earth Sci. Rev. 52 (4), 247–260. https://doi.org/10.1016/S0012-8252(00)00025-8.

Amiot, R., Lécuyer, C., Buffetaut, E., Fluteau, F., Legendre, S., Martineau, F., 2004. Latitudinal temperature gradient during the cretaceous upper campanian–middle maastrichtian: δ18O record of continental vertebrates. Earth Planet Sci. Lett. 226 (1–2), 255–272. https://doi.org/10.1016/j.epsl.2004.07.015.

Andreescu, I., Codrea, V., Lubenescu, V., Munteanu, T., Petculescu, A., Stiuca, E., Terzea, E., 2013. New developments in the upper pliocene-pleistocene stratigraphic units of the dacian basin (eastern paratethys), Romania. Quat. Int. 284, 15–29. https://doi.org/10.1016/j.quaint.2012.02.009.

Araguás-Araguás, L., Froehlich, K., Rozanski, K., 2000. Deuterium and oxygen-18 isotope composition of precipitation and atmospheric moisture. Hydrol. Process. 14 (8), 1341–1355. https://doi.org/10.1002/1099-1085(20000615)14:8<1341::aid-hyp983>3.0.co;2-z.

Araguas-Araguas, L.J., Diaz Teijeiro, M.F., 2005. Isotope Composition of Precipitation and Water Vapour in the Iberian Peninsula, vols. 1011–4289. International Atomic Energy Agency (IAEA), 92-0-105305-3.

Arppe, L., Karhu, J.A., 2010. Oxygen isotope values of precipitation and the thermal climate in Europe during the middle to late Weichselian ice age. Quat. Sci. Rev. 29 (9–10), 1263–1275. https://doi.org/10.1016/j.quascirev.2010.02.013.

Arppe, L., Karhu, J.A., 2006. Implications for the Late Pleistocene climate in Finland and adjacent areas from the isotopic composition of mammoth skeletal remains. Palaeogeogr. Palaeoclimatol. Palaeoecol. 231 (3–4), 322–330. https://doi.org/10.1016/j.palaeo.2005.08.007.

Ayliffe, L.K., Chivas, A.R., Leakey, M.G., 1994. The retention of primary oxygen isotope compositions of fossil elephant skeletal phosphate. Geochem. Cosmochim. Acta 58 (23), 5291–5298. https://doi.org/10.1016/0016-7037(94)90312-3.

Ayliffe, L.K., Lister, A.M., Chivas, A.R., 1992. The preservation of glacial-interglacial climatic signatures in the oxygen isotopes of elephant skeletal phosphate. Palaeogeogr. Palaeoclimatol. Palaeoecol. 99, 179–191. https://doi.org/10.1016/0031-0182(92)90014-v.

Bakker, E.S., Gill, J.L., Johnson, C.N., Vera, F.W.M., Sandom, C.J., Asner, G.P., Svenning, J.-C., 2016. Combining paleo-data and modern exclosure experiments to assess the impact of megafauna extinctions on woody vegetation. Proc. Natl. Acad. Sci. Unit. States Am. 113 (4), 847–855. https://doi.org/10.1073/pnas.1502545112.

Ballantyne, A.P., Rybczynski, N., Baker, P.A., Harington, C.R., White, D., 2006. Pliocene Arctic temperature constraints from the growth rings and isotopic composition of fossil larch. Palaeogeogr. Palaeoclimatol. Palaeoecol. 242 (3–4), 188–200. https://doi.org/10.1016/j.palaeo.2006.05.016.

Bartoli, G., Sarnthein, M., Weinelt, M., Erlenkeuser, H., Garbe-Schönberg, D., Lea, D.W., 2005. Final closure of Panama and the onset of northern hemisphere glaciation. Earth Planet Sci. Lett. 237 (1–2), 33–44. https://doi.org/10.1016/j.epsl.2005.06.020.

Bassett, D., Macleod, K.G., Miller, J.F., Ethington, R.L., 2007. Oxygen isotopic composition of biogenic phosphate and the temperature of Early Ordovician seawater. Palaios 22 (1), 98–103. https://doi.org/10.2110/palo.2005.p05-089r, 6.

Bertini, A., 2001. Pliocene climatic cycles and altitudinal forest development from 2.7 Ma in the Northern Apennines (Italy): evidence from the pollen record of the Stirone section (~ 5.1 to ~ 2.2 Ma). Geobios 34 (3), 253–265. https://doi.org/10.1016/S0016-6995(01)80074-7.

Bertini, A., 2010. Pliocene to Pleistocene palynoflora and vegetation in Italy: state of the art. Quat. Int. 225 (1), 5–24. https://doi.org/10.1016/j.quaint.2010.04.025.

Bocherens, H., Pacaud, G., Lazarev, P.A., Mariotti, A., 1996. Stable isotope abundances (C-13, N-15) in collagen and soft tissues from Pleistocene mammals from Yakutia: implications for the palaeobiology of the Mammoth Steppe. Palaeogeogr. Palaeoclimatol. Palaeoecol. 126, 31–44. https://doi.org/10.1016/s0031-0182(96)00068-5.

Bœuf, O., 1997. A propos de Chilhac, Senèze, Blassac-la-Girondie (Haute-Loire), gisements du Pliocène terminal, leur intérêt biochronologique. In: Aguilar, J.P., et al. (Eds.), European Neogene Mammal Chronology, Actes du Congrès Biochrom'97. In: Bons, M.J., Michaux, M.J. (Eds.), Mémoires et Travaux de l'Ecole Pratique des Hautes Etudes de Montpellier, 21. Dépot légal : Montpellier, pp. 661–668.

Bohn, U., Neuhäusl, R., , unter Mitarbeit von/with contributions by Gollub, G., Hettwer, C., Neuhäuslová, Z., Raus, Th, Schlüter, H., Weber, H., 2000/2003. In: Karte der natürlichen Vegetation Europas/Map of the Natural Vegetation of Europe. Maßstab/Scale 1 : 2 500 000. Münster (Landwirtschaftsverlag).

Boivin, P., Barbet, P., Boeuf, O., Devouard, B., Besson, J.-C., Hénot, J.-M., Devidal, J.-L., Constantin, C., Charles, L., 2010. Geological setting of the lower Pleistocene fossil deposits of Chilhac (Haute-Loire, France). Quat. Int. 223 (Suppl. C), 107–115. https://doi.org/10.1016/j.quaint.2009.12.010.

Brierley, C.M., Fedorov, A.V., Liu, Z., Herbert, T.D., Lawrence, K.T., LaRiviere, J.P., 2009. Greatly expanded tropical warm pool and weakened hadley circulation in the early pliocene. Science 323 (5922), 1714–1718. https://doi.org/10.1126/science.1167625.

Bruhl, J.J., Wilson, K.L., 2007. Towards a comprehensive survey of C3 and C4 photosynthetic pathways in cyperaceae. Aliso 23, 99e148. http://scholarship.claremont.edu/aliso/vol23/iss1/11.

Bryant, J.D., Froelich, P.N., 1995. A model of oxygen-isotope fractionation in body-water of large mammals. Geochem. Cosmochim. Acta 59, 4523–4537. https://doi.org/10.1016/0016-7037(95)00250-4.

Bryant, J.D., Koch, P.L., Froelich, P.N., Showers, W.J., Genna, B.J., 1996. Oxygen isotope partitioning between phosphate and carbonate in mammalian apatite. Geochem. Cosmochim. Acta 60 (24), 5145–5148. https://doi.org/10.1016/S0016-7037(96)00308-0.

Cerling, T.E., Harris, J.M., 1999. Carbon isotope fractionation between diet and bioapatite in ungulate mammals and implications for ecological and paleoecological studies. Oecologia 120, 347–363. https://doi.org/10.1007/s004420050868.

Cerling, T.E., Harris, J.M., Leakey, M.G., 1999. Browsing and grazing in elephants: the isotope record of modern and fossil proboscideans. Oecologia 120 (3), 364–374. https://doi.org/10.1007/s004420050869.

Chillón, B.S., Alberdi, M.T., Leone, G., Bonadonna, F.P., Stenni, B., Longinelli, A., 1994. Oxygen isotopic composition of fossil equid tooth and bone phosphate: an archive of difficult interpretation. Palaeogeogr. Palaeoclimatol. Palaeoecol. 107 (3), 317–328. https://doi.org/10.1016/0031-0182(94)90103-1.

Cirilli, O., Bernor, R., Rook, L., 2021. New insights on the early Pleistocene equids from roca-neyra (France, central Europe): implications for the hipparion LAD and the Equus FAD in Europe. J. Paleontol. 95 (2), 406–425. https://doi.org/10.1017/jpa.2020.99.

Combes, C., Cazalbou, S., Rey, C., 2016. Apatite biominerals. Minerals 6 (2), 34. https://doi.org/10.3390/min6020034.

Combourieu-Nebout, N., Bertini, A., Russo-Ermolli, E., Peyron, O., Klotz, S., Montade, V., Fauquette, S., Allen, J., Fusco, F., Goring, S., Huntley, B., Joannin, S., Lebreton, V., Magri, D., Martinetto, E., Orain, R., Sadori, L., 2015. Climate changes in the central Mediterranean and Italian vegetation dynamics since the Pliocene. Rev. Palaeobot. Palynol. 218, 127–147. https://doi.org/10.1016/j.revpalbo.2015.03.001.

Croitoru, A.-E., Piticar, A., Dragotă, C.S., Burada, D.C., 2013. Recent changes in reference evapotranspiration in Romania. Global Planet. Change 111, 127–136. https://doi.org/10.1016/j.gloplacha.2013.09.004.

Crowley, B.E., Wheatley, P.V., 2014. To bleach or not to bleach? Comparing treatment methods for isolating biogenic carbonate. Chem. Geol. 381, 234–242. https://doi.org/10.1016/j.chemgeo.2014.05.006.

Csank, A.Z., Patterson, W.P., Eglington, B.M., Rybczynski, N., Basinger, J.F., 2011a. Climate variability in the Early Pliocene Arctic: annually resolved evidence from stable isotope values of sub-fossil wood, Ellesmere Island, Canada. Palaeogeogr. Palaeoclimatol. Palaeoecol. 308, 339–349. https://doi.org/10.1016/j.palaeo.2011.05.038.

Csank, A.Z., Tripati, A.K., Patterson, W.P., Eagle, R.A., Rybczynski, N., Ballantyne, A.P., Eiler, J.M., 2011b. Estimates of Arctic land surface temperatures during the early Pliocene from two novel proxies. Earth Planet Sci. Lett. 304 (3–4), 291–299. https://doi.org/10.1016/j.epsl.2011.02.030.

Dansgaard, W., 1964. Stable isotopes in precipitation. Tellus 16 (4), 436–468. https://doi.org/10.1111/j.2153-3490.1964.tb00181.x.

De Bruijn, H., Daams, R., Daxner-Höck, G., Fahlbusch, V., Ginsburg, L., Mein, P., Morales, J., 1992. Report of the RCMNS working group on fossil mammals. Reisensburg 1990. Newsl. Stratigr. 26, 65–118.

De Schepper, S., Gibbard, P.L., Salzmann, U., Ehlers, J., 2014. A global synthesis of the marine and terrestrial evidence for glaciation during the Pliocene Epoch. Earth Sci. Rev. 135, 83–102. https://doi.org/10.1016/j.earscirev.2014.04.003.

De Schepper, S., Groeneveld, J., Naafs, B.D.A., Van Renterghem, C., Hennissen, J., Head, M.J., Louwye, S., Fabian, K., 2013. Northern hemisphere glaciation during the globally warm early late pliocene. PLoS One 8 (12). https://doi.org/10.1371/journal.pone.0081508.

Dettman, D.L., Kohn, M.J., Quade, J., Ryerson, F.J., Ojha, T.P., Hamidullah, S., 2001. Seasonal stable isotope evidence for a strong Asian monsoon throughout the past 10.7 m.y. Geology 29, 31e34. https://doi.org/10.1130/0091-7613(2001).

Domingo, L., Barroso-Barcenilla, F., Cambra-Moo, O., 2015. Seasonality and paleoecology of the late cretaceous multi-taxa vertebrate assemblage of "lo hueco" (central eastern Spain). PLoS One 10 (3), e0119968. https://doi.org/10.1371/journal.pone.0119968.

Domingo, L., Koch, P.L., Hernandez Fernandez, M., Fox, D.L., Domingo, M.S., Teresa Alberdi, M., 2013. Late Neogene and early quaternary paleoenvironmental and paleoclimatic conditions in southwestern Europe: isotopic analyses on mammalian taxa. PLoS One 8. https://doi.org/10.1371/journal.pone.0063739.

Domingo, L., Tomassini, R.L., Montalvo, C.I., San-Pérez, D., Alberdi, M.T., 2020. The Great American Biotic Interchange revisited: a new perspective from the stable isotope record of Argentine Pampas fossil mammals. Sci. Rep. 10, 1608. https://doi.org/10.1038/s41598-020-58575-6.

Doughty, C.E., Faurby, S., Svenning, J.C., 2016. The impact of the megafauna extinctions on savanna woody cover in South America. Ecography 39 (2), 213–222. https://doi.org/10.1111/ecog.01593.

Dowsett, H., Barron, J., Poore, R., 1996. Middle Pliocene sea surface temperatures: a global reconstruction. Mar. Micropaleontol. 27, 13–25. https://doi.org/10.1016/0377-8398(95)00050-X.

Dowsett, H., Robinson, M., Haywood, A.M., Salzmann, U., Hill, D., Sohl, L.E., Chandler, M., Williams, M., Foley, K., Stoll, D.K., 2010. The PRISM3D paleoenvironmental reconstruction. Stratigraphy 7 (2–3), 123–139.

Dowsett, H.J., Foley, K.M., Stoll, D.K., Chandler, M.A., Sohl, L.E., Bentsen, M., Otto-Bliesner, B.L., Bragg, F.J., Chan, W.L., Contoux, C., Dolan, A.M., Haywood, A.M., Jonas, J.A., Jost, A., Kamae, Y., Lohmann, G., Lunt, D.J., Nisancioglu, K.H., Abe-Ouchi, A., Ramstein, G., Riesselman, C.R., Robinson, M.M., Rosenbloom, N.A., Salzmann, U., Stepanek, C., Strother, S.L., Ueda, H., Yan, Q., Zhang, Z.S., 2013. sea surface temperature of the mid-piacenzian ocean: a data-model comparison. Sci. Rep. 3. https://doi.org/10.1038/srep02013.

Drucker, D.G., Bridault, A., Hobson, K.A., Szuma, E., Bocherens, H., 2008. Can carbon-13 in large herbivores reflect the canopy effect in temperate and boreal ecosystems? Evidence from modern and ancient ungulates. Palaeogeogr. Palaeoclimatol. Palaeoecol. 266 (1–2), 69–82. https://doi.org/10.1016/j.palaeo.2008.03.020.

Edwards, E.J., Osborne, C.P., Strömberg, C.A.E., Smith, S.A., 2010. The origins of C_4 grasslands: integrating evolutionary and ecosystem science. Science 328 (5978), 587–591. https://doi.org/10.1126/science.1177216.

Ehleringer, J.R., Monson, R.K., 1993. Evolutionary and ecological aspects of photosynthetic pathway variation. Annu. Rev. Ecol. Systemat. 24, 411–439.

Elias, S.A., Matthews Jr., J.V., 2002. Arctic North American seasonal temperatures from the latest Miocene to the Early Pleistocene, based on mutual climatic range analysis of fossil beetle assemblages. Can. J. Earth Sci. 39 (6), 911–920. https://doi.org/10.1139/e01-096.

Eronen, J.T., Rook, L., 2004. The Mio-Pliocene European primate fossil record: dynamics and habitat tracking. J. Hum. Evol. 47 (5), 323–341. https://doi.org/10.1016/j.jhevol.2004.08.003.

ESRI, 2021. World elevation TopoBathy. March 19, 2021. https://www.arcgis.com/home/item.html?id=c753e5bfadb54d46b69c3e68922483bc.

Faith, J.T., 2018. Paleodietary change and its implications for aridity indices derived from $\delta^{18}O$ of herbivore tooth enamel. Palaeogeogr. Palaeoclimatol. Palaeoecol. 490, 571–578. https://doi.org/10.1016/j.palaeo.2017.11.045.

Farquhar, G.D., Ehleringer, J.R., Hubick, K.T., 1989. Carbon isotope discrimination and photosynthesis. Annu. Rev. Plant Physiol. Plant Mol. Biol. 40 (1), 503–537. https://doi.org/10.1146/annurev.pp.40.060189.002443.

Fauquette, S., Bertini, A., 2003. Quantification of the northern Italy Pliocene climate from pollen data: evidence for a very peculiar climate pattern. Boreas 32 (2), 361–369. https://doi.org/10.1080/03009480310002235.

Fauquette, S., Guiot, J., Suc, J.-P., 1998. A method for climatic reconstruction of the Mediterranean Pliocene using pollen data. Palaeogeogr. Palaeoclimatol. Palaeoecol. 144 (1), 183–201. https://doi.org/10.1016/S0031-0182(98)00083-2.

Fauquette, S., Suc, J.P., Bertini, A., Popescu, S.M., Warny, S., Taoufiq, N.B., Villa, M.J.P., Chikhi, H., Feddi, N., Subally, D., Clauzon, G., Ferrier, J., 2006. How much did climate force the Messinian salinity crisis? Quantified climatic conditions from pollen records in the Mediterranean region. Palaeogeogr. Palaeoclimatol. Palaeoecol. 238 (1–4), 281–301. https://doi.org/10.1016/j.palaeo.2006.03.029.

Fauquette, S., Suc, J.P., Guiot, J., Diniz, F., Feddi, N., Zheng, Z., Bessais, E., Drivaliari, A., 1999. Climate and biomes in the west mediterranean area during the pliocene. Palaeogeogr. Palaeoclimatol. Palaeoecol. 152 (1–2), 15–36. https://doi.org/10.1016/s0031-0182(99)00031-0.

Fejfar, O., Heinrich, W.-D., Lindsay, E.H., 1998. Updating the Neogene rodent biochronology in Europe. Meded. Ned. Inst. Toegepaste Geowetenschappen TNO 60, 533e554.

Feranec, R.S., MacFadden, B.J., 2006. Isotopic discrimination of resource partitioning among ungulates in C-3-dominated communities from the Miocene of Florida and California. Paleobiology 32, 191–205. https://doi.org/10.1666/05006.1.

Fortelius, M., Eronen, J., Jernvall, J., Liu, L.P., Pushkina, D., Rinne, J., Tesakov, A., Vislobokova, I., Zhang, Z.Q., Zhou, L.P., 2002. Fossil mammals resolve regional patterns of Eurasian climate change over 20 million years. Evol. Ecol. Res. 4 (7), 1005–1016.

Fortelius, M., Eronen, J., Liu, L.P., Pushkina, D., Tesakov, A., Vislobokova, I., Zhang, Z.Q., 2006. Late Miocene and Pliocene large land mammals and climatic changes in Eurasia. Palaeogeogr. Palaeoclimatol. Palaeoecol. 238 (1–4), 219–227. https://doi.org/10.1016/j.palaeo.2006.03.042.

Fortelius, M., Mazza, P., Sala, B., 1993. Stephanorhinus (mammalia: Rhinocerotidae) of the western European Pleistocene, with a revision of S. etruscus (Falconer, 1868) 80, 63–155.

Fricke, H.C., Clyde, W.C., O'Neil, J.R., 1998. Intra-tooth variations in delta O-18 (PO4) of mammalian tooth enamel as a record of seasonal variations in continental climate variables. Geochem. Cosmochim. Acta 62 (11), 1839–1850. https://doi.org/10.1016/s0016-7037(98)00114-8.

Fricke, H.C., O'Neil, J.R., 1996. Inter- and intra-tooth variation in the oxygen isotope composition of mammalian tooth enamel phosphate: implications for palaeoclimatological and palaeobiological research. Palaeogeogr. Palaeoclimatol. Palaeoecol. 126, 91–99. https://doi.org/10.1016/S0031-0182(96)00072-7.

García-Alix, A., 2015. A multiproxy approach for the reconstruction of ancient continental environments. The case of the Mio–Pliocene deposits of the Granada Basin (southern Iberian Peninsula). Global Planet. Change 131, 1–10. https://doi.org/10.1016/j.gloplacha.2015.04.005.

GEBCO Compilation Group, 2020. GEBCO 2020 Grid. https://doi.org/10.5285/a29c5465-b138-234d-e053-6c86abc040b9.

Genty, D., Labuhn, I., Hoffmann, G., Danis, P.A., Mestre, O., Bourges, F., Wainer, K., Massault, M., Van Exter, S., Régnier, E., Orengo, P., Falourd, S., Minster, B., 2014. Rainfall and cave water isotopic relationships in two South-France sites. Geochem. Cosmochim. Acta 131 (Suppl. C), 323–343. https://doi.org/10.1016/j.gca.2014.01.043.

Giustini, F., Brilli, M., Patera, A., 2016. Mapping oxygen stable isotopes of precipitation in Italy. J. Hydrol.: Reg. Stud. 8 (Suppl. C), 162–181. https://doi.org/10.1016/j.ejrh.2016.04.001.

González-Guarda, E., Petermann-Pichincura, A., Tornero, C., Domingo, L., Agustí, J., Pino, M., Abarzúa, A.M., Capriles, J.M., Villavicencio, N.A., Labarca, R., Tolorza, V., Sevilla, P., Rivals, F., 2018. Multiproxy evidence for leaf-browsing and closed habitats in extinct proboscideans (Mammalia, Proboscidea) from Central Chile. Proc. Natl. Acad. Sci. Unit. States Am. 115 (37), 9258–9263. https://doi.org/10.1073/pnas.1804642115.

Groeneveld, J., Hathorne, E.C., Steinke, S., DeBey, H., Mackensen, A., Tiedemann, R., 2014. Glacial induced closure of the Panamanian gateway during marine isotope stages (MIS) 95–100 (~2.5 Ma). Earth Planet Sci. Lett. 404, 296–306. https://doi.org/10.1016/j.epsl.2014.08.007.

Guérin, C., 1972. Une nouvelle espèce de Rhinocéros (Mammalia, Perissodactyla) à Vialette (Haute-Loire, France) et dans d'autres gisements du Villafranchien Inférieur Européen: dicerorhinus jeanvireti n. sp. Doc. Lab. Geol. Fac. Sci Lyon 49, 53–161.

Guérin, C., 1980. Les rhinocéros (Mammalia, Perissodactyla) du Miocéne terminal au Pléistocéne supérieur en Europe occidentale. Comparaison avec les espéces actuelles. Doc. Lab. Geol. Fac. Sci. Lyon 79, 1–1183.

Guérin, C., Faure, M., Argant, A., Argant, J., Cregut-Bonnoure, E., Debard, E., Delson, E., Eisenmann, V., Hugueney, M., Limondin-Lozouet, N., Martin-Suarez, E., Mein, P., Mourer-Chauvire, C., Parenti, F., Pastre, J.F., Sen, S., Valli, A., 2004. The Late Pliocene site of Saint-Vallier (Drome, France): synthesis of

biostratigraphic and palaeoecological conclusions. Geobios 37, S349–S360. https://doi.org/10.1016/s0016-6995(04)80023-8.
Hably, L., Kvaček, Z., 1998. Pliocene mesophytic forests surrounding crater lakes in western Hungary. Rev. Palaeobot. Palynol. 101 (1), 257–269. https://doi.org/10.1016/S0034-6667(97)00077-8.
Haiduc, B.S., Răţoi, B.G., Semprebon, G.M., 2018. Dietary reconstruction of Plio-Pleistocene proboscideans from the Carpathian Basin of Romania using enamel microwear. Quat. Int. 467, 222–229. https://doi.org/10.1016/j.quaint.2018.01.039.
Hartman, G., Bar-Yosef, O., Brittingham, A., Grosman, L., Munro, N.D., 2016. Hunted gazelles evidence cooling, but not drying, during the Younger Dryas in the southern Levant. In: Proceedings of the National Academy of Sciences, p. 19862. https://doi.org/10.1073/pnas.1519862113, 2015.
Hatvani, I.G., Erdélyi, D., Vreča, P., Kern, Z., 2020. Analysis of the spatial distribution of stable oxygen and hydrogen isotopes in precipitation across the iberian Peninsula. Water 12 (2), 481. https://doi.org/10.3390/w12020481.
Hayes, J.M., 2001. Fractionation of carbon and hydrogen isotopes in biosynthetic processes. Rev. Mineral. Geochem. 43, 225–277. https://doi.org/10.2138/gsrmg.43.1.225.
Haywood, A.M., Hill, D.J., Dolan, A.M., Otto-Bliesner, B.L., Bragg, F., Chan, W.L., Chandler, M.A., Contoux, C., Dowsett, H.J., Jost, A., Kamae, Y., Lohmann, G., Lunt, D.J., Abe-Ouchi, A., Pickering, S.J., Ramstein, G., Rosenbloom, N.A., Salzmann, U., Sohl, L., Stepanek, C., Ueda, H., Yan, Q., Zhang, Z., 2013. Large-scale features of pliocene climate: results from the pliocene model intercomparison project. Clim. Past 9 (1), 191–209. https://doi.org/10.5194/cp-9-191-2013.
Haywood, A.M., Valdes, P.J., Sellwood, B.W., 2002. Magnitude of climate variability during middle Pliocene warmth: a palaeoclimate modelling study. Palaeogeogr. Palaeoclimatol. Palaeoecol. 188, 1–24. https://doi.org/10.1016/S0031-0182(02)00506-0.
Hilgen, F., Lourens, L., Van Dam, J.A., Beu, A., Boyes, A.F., Cooper, R., Krijgsman, W., Ogg, J., Piller, W., Wilson, D., 2012. The Neogene Period 1, 923–978. https://doi.org/10.1016/B978-0-444-59425-9.00029-9.
Hill, D.J., Csank, A.Z., Dolan, A.M., Lunt, D.J., 2011. Pliocene climate variability: northern Annular Mode in models and tree-ring data. Palaeogeogr. Palaeoclimatol. Palaeoecol. 309, 118–127. https://doi.org/10.1016/j.palaeo.2011.04.003.
Holko, L., Dóša, M., Michalko, J., Šanda, M., 2012. Isotopes of oxygen-18 and deuterium in precipitation in Slovakia/Izotopy kyslíka-18 A deutéria v zrážkach na Slovensku. https://doi.org/10.2478/v10098-012-0023-2, 60, 4, 265.
Horvatinčić, N., Krajcar Bronić, I., Barešić, J., Obelić, B., Vidič, S., 2005. Tritium and Stable Isotope Distribution in the Atmosphere at the Coastal Region of Croatia. International Atomic Energy Agency (IAEA), 1011-4289 92-0-105305-3.
Iacumin, P., Bocherens, H., Mariotti, A., Longinelli, A., 1996. Oxygen isotope analyses of co-existing carbonate and phosphate in biogenic apatite: a way to monitor diagenetic alteration of bone phosphate? Earth Planet Sci. Lett. 142, 1–6. https://doi.org/10.1016/0012-821x(96)00093-3.
Janis, C., 2008. An Evolutionary History of Browsing and Grazing Ungulates, 195. Springer, Berlin, Heidelberg, pp. 21–45. https://doi.org/10.1007/978-3-540-72422-3_2.
Jeffers, E.S., Whitehouse, N.J., Lister, A., Plunkett, G., Barratt, P., Smyth, E., Lamb, P., Dee, M.W., Brooks, S.J., Willis, K.J., Froyd, C.A., Watson, J.E., Bonsall, M.B., 2018. Plant controls on Late Quaternary whole ecosystem structure and function. Ecol. Lett. 21 (6), 814–825. https://doi.org/10.1111/ele.12944.
Ji, Q., Luo, Z.-X., Yuan, C.-X., Wible, J.R., Zhang, J.-P., Georgi, J.A., 2002. The earliest known eutherian mammal. Nature 416 (6883), 816–822. https://doi.org/10.1038/416816a.
Jiménez-Moreno, G., Fauquette, S., Suc, J.-P., 2010. Miocene to Pliocene vegetation reconstruction and climate estimates in the Iberian Peninsula from pollen data. Rev. Palaeobot. Palynol. 162 (3), 403–415. https://doi.org/10.1016/j.revpalbo.2009.08.001.
Johnson, M.R., Geary, D.H., 2016. Stable isotope ecology of hippotherium from the late miocene pannonian basin system. Palaeogeogr. Palaeoclimatol. Palaeoecol. 459, 44–52. https://doi.org/10.1016/j.palaeo.2016.06.039.
Jost, A., Fauquette, S., Kageyama, M., Krinner, G., Ramstein, G., Suc, J.P., Violette, S., 2009. High resolution climate and vegetation simulations of the Late Pliocene, a model-data comparison over western Europe and the Mediterranean region. Clim. Past 5 (4), 585–606. https://doi.org/10.5194/cp-5-585-2009.
Kahlke, R.-D., Kaiser, T.M., 2011. Generalism as a subsistence strategy: advantages and limitations of the highly flexible feeding traits of Pleistocene Stephanorhinus hundsheimensis (Rhinocerotidae, Mammalia). Quat. Sci. Rev. 30 (17), 2250–2261. https://doi.org/10.1016/j.quascirev.2009.12.012.
Koch, P.L., 1998. Isotopic reconstruction of past continental environments. Annu. Rev. Earth Planet Sci. 26, 573–613. https://doi.org/10.1146/annurev.earth.26.1.573.
Koch, P.L., 2007. Isotopic study of the biology of modern and fossil vertebrates. In: Michener, R., Lajtha, K. (Eds.), Stable Isotopes in Ecology and Environmental Science, second ed. Blackwell Publishing, Boston, pp. 99–154.
Koch, P.L., Tuross, N., Fogel, M.L., 1997. The effects of sample treatment and diagenesis on the isotopic integrity of carbonate in biogenic hydroxylapatite. J. Archaeol. Sci. 24, 417–429. https://doi.org/10.1006/jasc.1996.0126.
Kocsis, L., Ozsvárt, P., Becker, D., Ziegler, R., Scherler, L., Codrea, V., 2014. Orogeny forced terrestrial climate variation during the late Eocene-early Oligocene in Europe. Geology 42 (8), 727–730. https://doi.org/10.1130/g35673.1.
Kohn, M.J., 1996. Predicting animal delta O-18: accounting for diet and physiological adaptation. Geochem. Cosmochim. Acta 60 (23), 4811–4829. https://doi.org/10.1016/s0016-7037(96)00240-2.
Kohn, M.J., 2010. Carbon isotope compositions of terrestrial C3 plants as indicators of (paleo)ecology and (paleo)climate. Proc. Natl. Acad. Sci. U. S. A 107, 19691–19695. https://doi.org/10.1073/pnas.1004933107.
Kohn, M.J., Cerling, T.E., 2002. Stable isotope compositions of biological apatite. Phosphates: Geochem. Geobiol. Mater. Imp. 48, 455–488. https://doi.org/10.2138/rmg.2002.48.12.
Kohn, M.J., Schoeninger, M.J., Barker, W.W., 1999. Altered states: effects of diagenesis on fossil tooth chemistry. Geochem. Cosmochim. Acta 63 (18), 2737–2747. https://doi.org/10.1016/s0016-7037(99)00208-2.
Kolodny, Y., Luz, B., Navon, O., 1983. Oxygen isotope variations in phosphate of biogenic apatites, I. Fish bone apatite—rechecking the rules of the game. Earth Planet Sci. Lett. 64 (3), 398–404. https://doi.org/10.1016/0012-821X(83)90100-0.
Kovács, J., Moravcová, M., Újvari, G., Pintér, A.G., 2012. Reconstructing the paleoenvironment of East Central Europe in the Late Pleistocene using the oxygen and carbon isotopic signal of tooth in large mammal remains. Quat. Int. 276, 145–154. https://doi.org/10.1016/j.quaint.2012.04.009.
Kovács, J., Németh, K., Szabó, P., Kocsis, L., Kereszturi, G., Újvári, G., Vennemann, T., 2020. Volcanism and paleoenvironment of the pula maar complex: a pliocene terrestrial fossil site in Central Europe (Hungary). Palaeogeogr. Palaeoclimatol. Palaeoecol. 537, 109398. https://doi.org/10.1016/j.palaeo.2019.109398.
Kovács, J., Szabó, P., Kocsis, L., Vennemann, T., Sabol, M., Gasparik, M., Virág, A., 2015. Pliocene and Early Pleistocene paleoenvironmental conditions in the Pannonian Basin (Hungary, Slovakia): stable isotope analyses of fossil proboscidean and perissodactyl teeth. Palaeogeogr. Palaeoclimatol. Palaeoecol. 440, 455–466. https://doi.org/10.1016/j.palaeo.2015.09.019.
Krivoruchko, K., Gribov, A., 2019. Evaluation of empirical Bayesian kriging. Spat. Stat. 32, 100368. https://doi.org/10.1016/j.spasta.2019.100368, 2019.
Lacombat, F., Abbazzi, L., Ferretti, M.P., Martínez-Navarro, B., Moullé, P.-E., Palombo, M.-R., Rook, L., Turner, A., Valli, A.M.F., 2008. New data on the early villafranchian fauna from vialette (Haute-Loire, France) based on the collection of the crozatier Museum (le puy-en-velay, haute-loire, France). Quat. Int. 179 (1), 64–71. https://doi.org/10.1016/j.quaint.2007.09.005.
Lacombat, F., Mörs, T., 2008. The northernmost occurrence of the rare Late Pliocene rhinoceros Stephanorhinus jeanvireti (Mammalia, Perissodactyla). Neues Jahrbuch Fur Geologie Und Palaontologie-Abhandlungen 249 (2), 157–165. https://doi.org/10.1127/0077-7749/2008/0249-0157.
LaRiviere, J.P., Ravelo, A.C., Crimmins, A., Dekens, P.S., Ford, H.L., Lyle, M., Wara, M.W., 2012. Late Miocene decoupling of oceanic warmth and atmospheric carbon dioxide forcing. Nature 486 (7401), 97–100. https://doi.org/10.1038/nature11200.
Lee-Thorp, J.A., van der Merwe, N.J., 1987. Carbon isotope analysis of fossil bone apatite. South Afr. J. Sci. 83 (11), 712–715.
Lee-Thorp, J.A., Sealy, J.C., van der Merwe, N.J., 1989. Stable carbon isotope ratio differences between bone collagen and bone apatite, and their relationship to diet. J. Archaeol. Sci. 16 (6), 585–599. https://doi.org/10.1016/0305-4403(89)90024-1.
Levin, N.E., Cerling, T.E., Passey, B.H., Harris, J.M., Ehleringer, J.R., 2006. A stable isotope aridity index for terrestrial environments. Proc. Natl. Acad. Sci. U. S. A 103 (30), 11201–11205. https://doi.org/10.1073/pnas.0604719103.
Longinelli, A., 1966. Ratios of oxygen-18 : oxygen-16 in phosphate and carbonate from living and fossil marine organisms. Nature 211 (5052), 923–927. https://doi.org/10.1038/211923a0.
Longinelli, A., 1984. Oxygen isotopes in mammal bone phosphate: a new tool for paleohydrological and paleoclimatological research? Geochem. Cosmochim. Acta 48 (2), 385–390. https://doi.org/10.1016/0016-7037(84)90259-x.
Longinelli, A., Selmo, E., 2003. Isotopic composition of precipitation in Italy: a first overall map. J. Hydrol. 270 (1), 75–88. https://doi.org/10.1016/0016-7037(84)90259-x.
Luz, B., Kolodny, Y., Horowitz, M., 1984. Fractionation of oxygen isotopes between mammalian bone phosphate and environmental drinking-water. Geochem. Cosmochim. Acta 48, 1689–1693. https://doi.org/10.1016/0016-7037(84)90338-7.
Luz, B., Cormie, A.B., Schwarcz, H.P., 1990. Oxigen isotope variations in phosphate of deer bones. Geochem. Cosmochim. Acta 54, 1723–1728. https://doi.org/10.1016/0016-7037(90)90403-8.
Mandić, O., Göhlich, U., Hrvatović, H., Mauch-Lenardić, J., Čvorović, B., Glamuzina, G., Radoš, D., 2013. New proboscidean site from the high karst dinarides in southern Bosnia and Herzegovina. In: Neogene to Quaternary Geological Evolution of Mediterranean, Paratethys and Black Sea, Istanbul, Regional Committee of Mediterranean Neogene Stratigraphy. 14th RCMNS Congress, Istanbul. Book of Abstracts, p. 189.
Martin, C., Bentaleb, I., Kaandorp, R., Iacumin, P., Chatri, K., 2008. Intra-tooth study of modern rhinoceros enamel δ18O: is the difference between phosphate and carbonate δ18O a sound diagenetic test? Palaeogeogr. Palaeoclimatol. Palaeoecol. 266, 183–189. https://doi.org/10.1016/j.palaeo.2008.03.039.
Martinelli, L.A., Devol, H.A., Victoria, R.L., Richey, J.E., 1991. Stable carbon isotope variation in C_3 and C_4 plants along the Amazon River. Nature 353, 57–59. https://doi.org/10.1038/353057a0.
Martinetto, E., Momohara, A., Bizzarri, R., Baldanza, A., Delfino, M., Esu, D., Sardella, R., 2017. Late persistence and deterministic extinction of "humid thermophilous plant taxa of East Asian affinity" (HUTEA) in southern Europe. Palaeogeogr. Palaeoclimatol. Palaeoecol. 467, 211–231. https://doi.org/10.1016/j.palaeo.2015.08.015.

Masson-Delmotte, V., Schulz, M., Abe-Ouchi, A., Beer, J., Ganopolski, A., González Rouco, J.F., Jansen, E., Lambeck, K., Luterbacher, J., Naish, T., Osborn, T., Otto-Bliesner, B., Quinn, T., Ramesh, R., Rojas, M., Shao, X., Timmermann, A., 2013. Information from paleoclimate archives. In: Stocker, T.F., Qin, D., Plattner, G.-K., Tignor, M., Allen, S.K., Boschung, J., Nauels, A., Xia, Y., Bex, V., Midgley, P.M. (Eds.), Climate Change 2013: the Physical Science Basis. Contribution of Working Group I to the Fifth Assessment Report of the Intergovernmental Panel on Climate Change. Cambridge University Press, Cambridge, United Kingdom and New York, NY, USA. https://www.ipcc.ch/report/ar5/wg1/.

Matson, S.D., Fox, D.L., 2010. Stable isotopic evidence for terrestrial latitudinal climate gradients in the Late Miocene of the Iberian Peninsula. Palaeogeogr. Palaeoclimatol. Palaeoecol. 287 (1), 28–44. https://doi.org/10.1016/j.palaeo.2009.12.010.

Mazza, P., 1988. The tuscan early Pleistocene rhinoceros dicerorhinus etruscus. Palaeontogr. Ital. 75, 1–87.

Mein, P., 1975. Résultats du groupe de travail des vertébrés: biozonation du Néogène méditerranéen à partir des mammifères. In: Senes, J. (Ed.), Report on Activity of the Regional Committee on Mediterranean Neogene Stratigraphy, Working Groups, pp. 77–81. Bratislava.

Metcalfe, J.Z., Longstaffe, F.J., 2012. Mammoth tooth enamel growth rates inferred from stable isotope analysis and histology. Quater. Res. 77, 424–432. https://doi.org/10.1016/j.yqres.2012.02.002.

Metcalfe, J.Z., Longstaffe, F.J., Jass, C.N., Zazula, G.D., Keddie, G., 2016. Taxonomy, location of origin and health status of proboscideans from Western Canada investigated using stable isotope analysis. J. Quat. Sci. 31 (2), 126–142. https://doi.org/10.1002/jqs.2849.

Meyers, S.R., Hinnov, L.A., 2010. Northern Hemisphere glaciation and the evolution of Plio-Pleistocene climate noise. Paleoceanography 25. https://doi.org/10.1029/2009pa001834.

Nomade, S., Pastre, J.F., Guillou, H., Faure, M., Guérin, C., Delson, E., Debard, E., Voinchet, P., Messager, E., 2014. 40Ar/39Ar constraints on some French landmark Late Pliocene to Early Pleistocene large mammalian paleofaunas: paleoenvironmental and paleoecological implications. Quat. Geochronol. 21, 2–15. https://doi.org/10.1016/j.quageo.2012.12.006.

O'Leary, M.H., 1988. Carbon isotopes in photosynthesis. Bioscience 38 (5), 328–336. https://doi.org/10.2307/1310735.

Oloo, T.W., Brett, R., Young, T.P., 1994. Seasonal variation in the feeding ecology of black rhinoceros (Diceros bicornis L.) in Laikipia, Kenya. Afr. J. Ecol. 32 (2), 142–157. https://doi.org/10.1111/j.1365-2028.1994.tb00565.x.

Oms, O., Dinarès-Turell, J., Agustí, J., M. Parés, J., 1999. Refinements of the European mammal biochronology from the magnetic polarity record of the plio–pleistocene zújar section, guadix-baza basin, SE Spain. Quater. Res. 51 (1), 94–103. https://doi.org/10.1006/qres.1998.2018.

Palombo, M.R., 2007. What is the boundary for the Quaternary period and Pleistocene epoch? The contribution of turnover patterns in large mammalian complexes from north-western Mediterranean to the debate. Quaternaire 18 (1), 35–53.

Paquette, J.-L., Médard, E., Poidevin, J.-L., Barbet, P., 2021. Precise dating of middle to late Villafranchian mammalian paleofaunae from the Upper Allier River valley (French Massif Central) using U–Pb geochronology on volcanic zircons. Quat. Geochronol. 65, 101198. https://doi.org/10.1016/j.quageo.2021.101198.

Passey, B.H., Robinson, T.F., Ayliffe, L.K., Cerling, T.E., Sponheimer, M., Dearing, M.D., Roeder, B.L., Ehleringer, J.R., 2005. Carbon isotope fractionation between diet, breath CO2, and bioapatite in different mammals. J. Archaeol. Sci. 32 (10), 1459–1470. https://doi.org/10.1016/j.jas.2005.03.015.

Pellegrini, M., Lee-Thorp, J.A., Donahue, R.E., 2011. Exploring the variation of the delta O-18(p) and delta O-18(c) relationship in enamel increments. Palaeogeogr. Palaeoclimatol. Palaeoecol. 310 (1–2), 71–83. https://doi.org/10.1016/j.palaeo.2011.02.023.

Pellegrini, M., Snoeck, C., 2016. Comparing bioapatite carbonate pre-treatments for isotopic measurements: Part 2 — impact on carbon and oxygen isotope compositions. Chem. Geol. 420, 88–96. https://doi.org/10.1016/j.chemgeo.2015.10.038.

Petronio, C., Bellucci, L., Martinetto, E., Pandolfi, L., Salari, L., 2011. Biochronology and palaeoenvironmental changes from the middle pliocene to the late Pleistocene in Central Italy. Geodiversitas 33 (3), 485–517. https://doi.org/10.5252/g2011n3a4.

Pontini, M.R., Bertini, A., 2000. Late Pliocene vegetation and climate in Central Italy: high-resolution pollen analysis from the Fosso Bianco succession (Tiberino Basin). Geobios 33 (5), 519–526. https://doi.org/10.1016/s0016-6995(00)80024-8.

Popov, S.V., Shcherba, I.G., Ilyina, L.B., Nevesskaya, L.A., Paramonova, N.P., Khondkarian, S.O., Magyar, I., 2006. Late miocene to pliocene palaeogeography of the paratethys and its relation to the mediterranean. Palaeogeogr. Palaeoclimatol. Palaeoecol. 238 (1), 91–106. https://doi.org/10.1016/j.palaeo.2006.03.020.

Pryor, A.J.E., Stevens, R.E., O'Connell, T.C., Lister, J.R., 2014. Quantification and propagation of errors when converting vertebrate biomineral oxygen isotope data to temperature for palaeoclimate reconstruction. Palaeogeogr. Palaeoclimatol. Palaeoecol. 412, 99–107. https://doi.org/10.1016/j.palaeo.2014.07.003.

Quade, J., Cerling, T.E., Barry, J.C., Morgan, M.E., Pilbeam, D.R., Chivas, A.R., Lee-Thorp, J.A., Van der Merwe, N.J., 1992. A 16-Ma record of paleodiet using carbon and oxygen isotopes in fossil teeth from Pakistan. Chem. Geol. 94 (3), 183–192. https://doi.org/10.1016/0168-9622(92)90011-x.

Radulescu, C., Samson, P.-M., Petculescu, A., Stiucă, E., 2003. Pliocene large mammals of Romania. Coloq. Paleontol. 1, 549–558.

Rivals, F., Julien, M.-A., Kuitems, M., Van Kolfschoten, T., Serangeli, J., Drucker, D.G., Bocherens, H., Conard, N.J., 2015. Investigation of equid paleodiet from Schöningen 13 II-4 through dental wear and isotopic analyses: archaeological implications. J. Hum. Evol. 89, 129–137. https://doi.org/10.1016/j.jhevol.2014.04.002.

Roger, S., Coulon, C., Thouveny, N., Féraud, G., Van Velzen, A., Fauquette, S., Cochemé, J.J., Prévot, M., Verosub, K.L., 2000. 40Ar/39Ar dating of a tephra layer in the Pliocene Senèze maar lacustrine sequence (French Massif Central): constraint on the age of the Réunion–Matuyama transition and implications on paleoenvironmental archives. Earth Planet Sci. Lett. 183 (3), 431–440. https://doi.org/10.1016/S0012-821X(00)00285-5.

Rook, L., Martínez-Navarro, B., 2010. Villafranchian: the long story of a Plio-Pleistocene European large mammal biochronologic unit. Quat. Int. 219 (1–2), 134–144. https://doi.org/10.1016/j.quaint.2010.01.007.

Rozanski, K., Araguás-Araguás, L., Gonfiantini, R., 1993. Isotopic patterns in modern global precipitation. In: Climate Change in Continental Isotopic Records. American Geophysical Union, pp. 1–36. https://doi.org/10.1029/GM078p0001.

Saarinen, J., Lister, A.M., 2016. Dental mesowear reflects local vegetation and niche separation in Pleistocene proboscideans from Britain. J. Quat. Sci. 31 (7), 799–808. https://doi.org/10.1002/jqs.2906.

Salzmann, U., Dolan, A.M., Haywood, A.M., Chan, W.-L., Voss, J., Hill, D.J., Abe-Ouchi, A., Otto-Bliesner, B., Bragg, F.J., Chandler, M.A., Contoux, C., Dowsett, H.J., Jost, A., Kamae, Y., Lohmann, G., Lunt, D.J., Pickering, S.J., Pound, M.J., Ramstein, G., Rosenbloom, N.A., Sohl, L., Stepanek, C., Ueda, H., Zhang, Z., 2013. Challenges in quantifying Pliocene terrestrial warming revealed by data–model discord. Nat. Clim. Change 3, 969. https://doi.org/10.1038/nclimate2008.

Salzmann, U., Williams, M., Haywood, A.M., Johnson, A.L.A., Kender, S., Zalasiewicz, J., 2011. Climate and environment of a Pliocene warm world. Palaeogeogr. Palaeoclimatol. Palaeoecol. 309 (1–2), 1–8. https://doi.org/10.1016/j.palaeo.2011.05.044.

Sánchez-Chillón, B.S., Alberdi, M.T., Leone, G., Bonadonna, F.P., Stenni, B., Longinelli, A., 1994. Oxygen isotopic composition of fossil equid tooth and bone phosphate: an archive of difficult interpretation. Palaeogeogr. Palaeoclimatol. Palaeoecol. 107 (3), 317–328. https://doi.org/10.1016/0031-0182(94)90103-1.

Scotese, C.R., 2016. PALEOMAP PaleoAtlas for GPlates and the PaleoData Plotter Program. PALEOMAP Project. http://www.earthbyte.org/paleomap-paleoatlas-for-gplates/.

Scotese, C.R., Wright, N., 2018. PALEOMAP Paleodigital Elevation Models (Paleo-DEMS) for the Phanerozoic PALEOMAP Project. https://www.earthbyte.org/paleodem-resourcescotese-and-wright-2018/.

Skrzypek, G., Sadler, R., Wiśniewski, A., 2016. Reassessment of recommendations for processing mammal phosphate δ18O data for paleotemperature reconstruction. Palaeogeogr. Palaeoclimatol. Palaeoecol. 446, 162–167. https://doi.org/10.1016/j.palaeo.2016.01.032.

Spötl, C., Vennemann, T.W., 2003. Continuous-flow isotope ratio mass spectrometric analysis of carbonate minerals. Rapid Commun. Mass Spectrom. 17, 1004–1006. https://doi.org/10.1002/rcm.1010.

Suc, J., Diniz, F., Leroy, S., Poumot, C., Bertini, A., Dupont, L., Clet, M., Bessais, E., Zheng, Z., Fauquette, S., 1995. Zanclean (~ brunssumian) to early piacenzian (~ early-middle reuverian) climate from 4 to 54 north latitude (west africa, west Europe and West mediterranean areas). Meded. Rijks Geol. Dienst 52, 43–56.

Sullivan, C.H., Krueger, H.W., 1981. Carbon isotope analysis of separate chemical phases in modern and fossil bone. Nature 292 (5821), 333–335. https://doi.org/10.1038/292333a0.

Szabó, P., Kocsis, L., Vennemann, T., Pandolfi, L., Kovács, J., Martinetto, E., Demény, A., 2017. Pliocene–Early Pleistocene climatic trends in the Italian Peninsula based on stable oxygen and carbon isotope compositions of rhinoceros and gomphothere tooth enamel. Quat. Sci. Rev. 157, 52–65. https://doi.org/10.1016/j.quascirev.2016.11.003.

Tafforeau, P., Bentaleb, I., Jaeger, J.-J., Martin, C., 2007. Nature of laminations and mineralization in rhinoceros enamel using histology and X-ray synchrotron microtomography: potential implications for palaeoenvironmental isotopic studies. Palaeogeogr. Palaeoclimatol. Palaeoecol. 246 (2–4), 206–227. https://doi.org/10.1016/j.palaeo.2006.10.001.

Tejada-Lara, J.V., MacFadden, B.J., Bermudez, L., Rojas, G., Salas-Gismondi, R., Flynn, J.J., 2018. Body mass predicts isotope enrichment in herbivorous mammals. Proc. Biol. Sci. 285, 20181020. https://doi.org/10.1098/rspb.2018.1020, 1881.

Tipple, B.J., Meyers, S.R., Pagani, M., 2010. Carbon isotope ratio of Cenozoic CO2: a comparative evaluation of available geochemical proxies. Paleoceanography 25. https://doi.org/10.1029/2009pa001851.

Trayler, R.B., Kohn, M.J., 2017. Tooth enamel maturation reequilibrates oxygen isotope compositions and supports simple sampling methods. Geochem. Cosmochim. Acta 198, 32–47. https://doi.org/10.1016/j.gca.2016.10.023.

Tudge, A.P., 1960. A method of analysis of oxygen isotopes in orthophosphate—its use in the measurement of paleotemperatures. Geochem. Cosmochim. Acta 18 (1), 81–93. https://doi.org/10.1016/0016-7037(60)90019-3.

Tütken, T., Furrer, H., Vennemann, T.W., 2007. Stable isotope compositions of mammoth teeth from Niederweningen, Switzerland: implications for the Late Pleistocene climate, environment, and diet. Quat. Int. 164–65, 139–150. https://doi.org/10.1016/j.quaint.2006.09.004.

Tütken, T., Kaiser, T.M., Vennemann, T., Merceron, G., 2013. Opportunistic feeding strategy for the earliest old world hypsodont equids: evidence from stable isotope and dental wear proxies. PLoS One 8. https://doi.org/10.1371/

journal.pone.0074463.
Tütken, T., Vennemann, T.W., Janz, H., Heimann, E.P.J., 2006. Palaeoenvironment and palaeoclimate of the Middle Miocene lake in the Steinheim Basin, SW Germany: a reconstruction from C, O, and Sr isotopes of fossil remains. Palaeogeogr. Palaeoclimatol. Palaeoecol. 241, 457–491. https://doi.org/10.1016/j.palaeo.2006.04.007.
van Dam, J.A., Reichart, G.J., 2009. Oxygen and carbon isotope signatures in late Neogene horse teeth from Spain and application as temperature and seasonality proxies. Palaeogeogr. Palaeoclimatol. Palaeoecol. 274 (1–2), 64–81. https://doi.org/10.1016/j.palaeo.2008.12.022.
van der Merwe, N.J., Medina, E., 1991. The canopy effect, carbon isotope ratios and foodwebs in amazonia. J. Archaeol. Sci. 18 (3), 249–259. https://doi.org/10.1016/0305-4403(91)90064-V.
Vennemann, T.W., Fricke, H.C., Blake, R.E., O'Neil, J.R., Colman, A., 2002. Oxygen isotope analysis of phosphates: a comparison of techniques for analysis of Ag3PO4. Chem. Geol. 185, 321–336. https://doi.org/10.1016/s0009-2541(01)00413-2.
Vodila, G., Palcsu, L., Futó, I., Szántó, Z., 2011. A 9-year record of stable isotope ratios of precipitation in Eastern Hungary: implications on isotope hydrology and regional palaeoclimatology. J. Hydrol. 400 (1), 144–153. https://doi.org/10.1016/j.jhydrol.2011.01.030.
Wang, Y., Cerling, T.E., 1994. A model of fossil tooth and bone diagenesis — implications for paleodiet reconstruction from stable isotopes. Palaeogeogr. Palaeoclimatol. Palaeoecol. 107 (3–4), 281–289. https://doi.org/10.1016/0031-0182(94)90100-7.
Woodard, S.C., Rosenthal, Y., Miller, K.G., Wright, J.D., Chiu, B.K., Lawrence, K.T., 2014. Antarctic role in northern hemisphere glaciation. Science 346 (6211), 847–851. https://doi.org/10.1126/science.1255586.
Yann, L.T., DeSantis, L.R.G., Haupt, R.J., Romer, J.L., Corapi, S.E., Ettenson, D.J., 2013. The application of an oxygen isotope aridity index to terrestrial paleoenvironmental reconstructions in Pleistocene North America. Paleobiology 39 (4), 576–590. https://doi.org/10.1666/12059.
Zazzo, A., Lecuyer, C., Mariotti, A., 2004a. Experimentally-controlled carbon and oxygen isotope exchange between bioapatites and water under inorganic and microbially-mediated conditions. Geochem. Cosmochim. Acta 68, 1–12. https://doi.org/10.1016/s0016-7037(03)00278-3.
Zazzo, A., Lecuyer, C., Sheppard, S.M.F., Grandjean, P., Mariotti, A., 2004b. Diagenesis and the reconstruction of paleoenvironments: a method to restore original delta O-18 values of carbonate and phosphate from fossil tooth enamel. Geochem. Cosmochim. Acta 68, 2245–2258. https://doi.org/10.1016/j.gca.2003.11.009.